Important Notice

UNIVERSITY OF CALGARY

Determination of Reservoir Characteristics

Using Geostatistical Analysis

by

Hong Xu

A THESIS

SUBMITTED TO THE FACULTY OF GRADUATE STUDIES

IN PARTIAL FULFILLMENT OF THE REQUIREMENTS FOR THE

DEGREE OF MASTER OF SCIENCE

GRADUATE PROGRAM IN GEOLOGY AND GEOPHYSICS

CALGARY, ALBERTA

JUNE, 2017

Abstract

Geostatistics offers a robust way to estimate the spatial distribution of reservoir properties. Geostatistical methods, such as kriging, cokriging, and sequential simulation have been applied to integrate well-log data and seismic attributes. However, conventional deterministic methods of geostatistics, kriging and cokriging often have difficulty identifying the characteristics of lithologic reservoirs because only one secondary attribute is incorporated. To decrease the uncertainty and improve the definition of the final estimate, two modified techniques, cokriging with multiple secondary attributes and block cokriging with multiple secondary attributes, are implemented. However, these deterministic methods can only provide one predicted result, which has trouble capturing the natural heterogeneity of reservoirs and assessing the uncertainty of the predicted map. To solve this issue, an improved stochastic technique, sequential simulation using multi-variable cokriging, is presented.

All these presented techniques are applied to real datasets. Case studies are presented to predict the thickness of the reservoir, total organic carbon, and porosity. The final predicted maps demonstrate that these methods can enhance the lateral resolution. Leave-one-out cross-validation is used to evaluate the construction models, and shows that the uncertainty of the estimate can be reduced due to the use of more seismic attributes than traditionally implemented, while still optimizing cross-validation.

Acknowledgements

I would like to first and foremost thank my supervisor, Dr. Kristopher Innanen, and my co-supervisor, Dr. Brian Russell. Dr. Russell was the first one I talked to about becoming a master's student in geophysics. His support changed my life. He not only opened the door of the geophysical world for me, but also walked with me throughout the whole experience. His wisdom and knowledge made my studies enjoyable and productive. Nobody can imagine how happy I was when Dr. Innanen took me as his student. I would really like to express my most sincere appreciation to Dr. Innanen for his leadership and guidance. It would not have been possible to complete my degree without his constant encouragement and incredible patience.

A special thank you to Jian Sun for helpful discussions and innovative suggestions in my research work. He was always there for me whenever I needed help.

I would like to thank Darren Schmidt for his invaluable support. I am grateful for his sharing of practical geophysical knowledge and experience with me.

I want to thank Dr. Larry Lines and Dr. Daniel Trad for being my thesis examiners. Special thanks to you, Dr. Lines, for changing your medical schedule for to accommodate my thesis oral exam time. Sincere thanks to Dr. Trad for teaching me the signal processing course.

Finally, I want to acknowledge my co-workers in the CGG Hampson-Russell division and the people in the CREWES project for supporting me.

Table of Contents

List of Figures and Illustrations

List of Symbols, Abbreviations and Nomenclature

Symbol	Definition
AVO	Amplitude Versus Offset
BCK	Block cokriging
LS	Least-squares
OCK	Ordinary cokriging
RMS	Root-mean-square
ROCK	Rescaled ordinary cokriging
SCK	Simple cokriging
SGS	Sequential Gaussian simulation
SGS_LS	SGS implemented by the LS method
SGS_ROCK	SGS implemented by the ROCK method
TOC	Total organic carbon

Chapter 1

Introduction

1.1 Introduction

Geostatistics can be regarded as a collection of numerical techniques that deal with the characterization of spatial attributes, employing primarily random models (Olea, 1999). Recently, geostatistics has become widely used in geoscience for reservoir characterization and modelling. The aim of geostatistics is to provide accurate estimates on unsampled locations with a quantification of the uncertainty. Geostatistical prediction differs from classical estimation because it relies on spatial relationships, such as variogram analysis. If there is a strong spatial correlation between random samples, then it is possible to estimate more precisely.

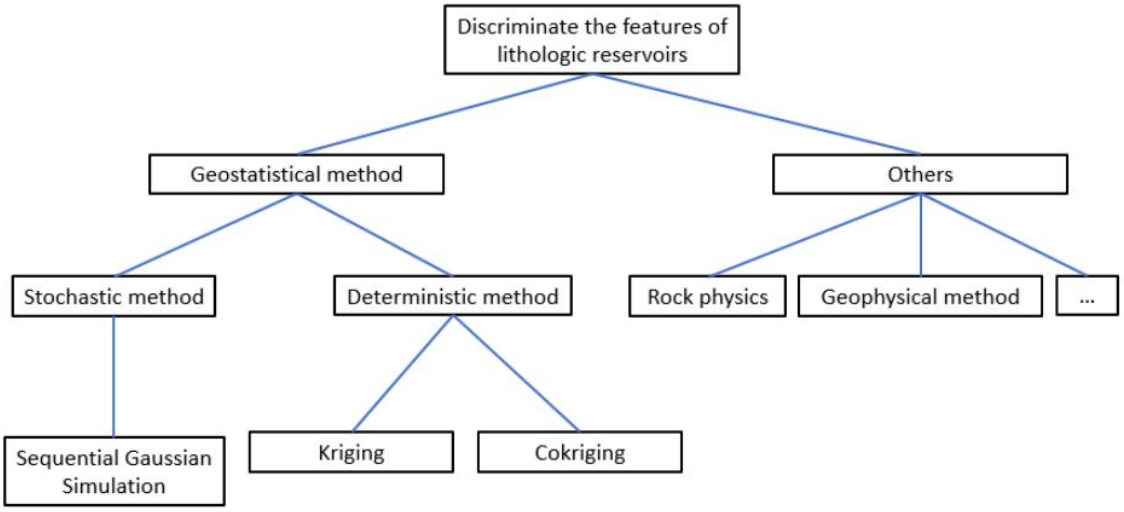

Figure 1.1: The family of geostatistics

The geostatistical approaches use spatial correlation to model the lateral variation of the reservoir properties (Ambrose, R.J., Hartman, R.C., Diaz Campos, M., Akkutlu, I.Y. and Sondergeld,

C., 2010). Techniques include geostatistical estimation (also called the deterministic method), such as kriging and cokriging; geostatistical simulation (also called the stochastic method), such as sequential Gaussian simulation (SGS) (Figure 1.1). Kriging can interpolate a value distributed on a random field at an unsampled location based on the sample values (primary variable) only at nearby locations (Doyen, P. M., 1988). Cokriging, an extension of kriging, reduces the smooth effects and provides specific prediction of the estimate by incorporating seismic data as a secondary variable, due to its more complete distribution. The seismic attribute has to be effective in order to introduce more geological information and is usually validated by its correlation with the primary variable. Cross-plot analysis can help to determine the correlation between primary and secondary variables. As deterministic methods, kriging and cokriging can only provide one predicted result, which may not have the capability to characterize heterogeneity in petroleum reservoirs.

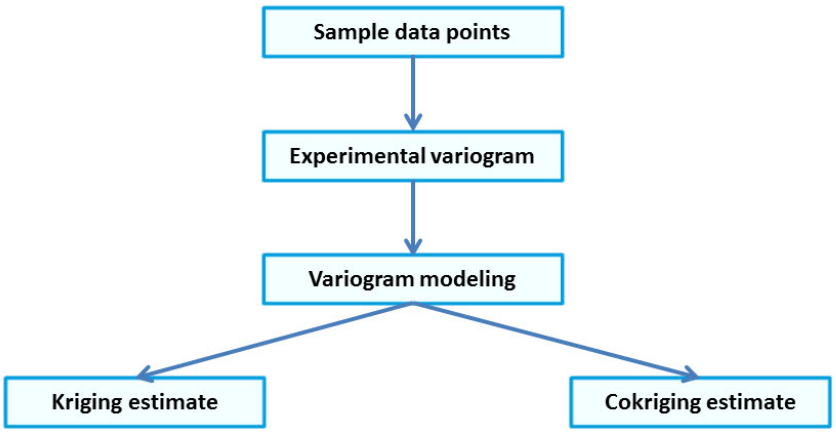

(a) The work-flow for geostatistical estimate

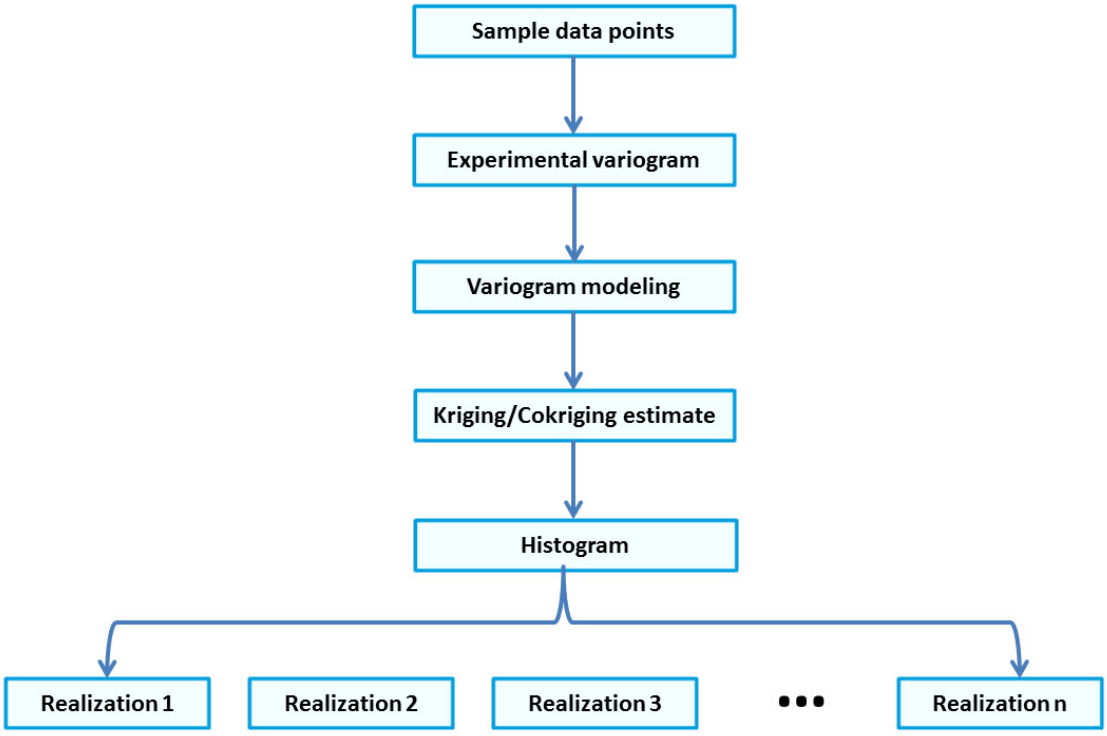

(b) The work-flow for geostatistical simulation

Figure 1.2: The work-flow for geostatistical methods

The stochastic simulation technique provides a series of equally valid and possible realizations that indirectly reflect the distribution of reservoir properties. Each realization is built by the mean and covariance estimated at each grid cell using kriging, cokriging, or a least-squares method. As

an additional benefit, the geostatistical simulation method has the ability to quantify the uncertainty of the estimation by generating a probability map. The work-flow for the geostatistical estimation and simulation are displayed in Figure 1.2 (a) and Figure 1.2(b).

One of the challenges in cokriging is that traditionally only a single secondary variable is used. To optimize the secondary variable in cokriging, many techniques have been proposed, such as multi-attribute analysis and super-secondary dataset method. However, both methods have limitations. The multi-attribute method assumes that there is high correlation between the estimated area and the well locations; the super-secondary dataset method assumes that all datasets must be a linear combination of each other.

In this thesis, to reduce these assumptions, three modified geostatistical methods, cokriging with multiple secondary variables in Chapter 5, block cokriging with multiple secondary attributes in Chapter 6, and sequential simulation using multi-variable cokriging in Chapter 7, are introduced and evaluated. These methods differ from traditional ones by introducing more than one secondary variable. It is beneficial to use multiple secondary variables to support the prediction because each secondary variable may have the unique information about the reservoir characteristics. In summary, the objective of this work is to present the modified techniques and evaluate their performance through applications using real datasets. Additionally, the traditional techniques are reviewed and described, including kriging in Chapter 2, leave-one-out cross-validation in Chapter 3, and cokriging in Chapter 4.

1.2 Hardware and software

All the work in this thesis has been done on the desktop computer provided by the CREWES project of the Department of Geology and Geophysics at the University of Calgary. The programming code was developed by Matlab in Chapter 5, 6, and 7 where CGG Hampson-Russell software has been employed to prepare well-log data (primary variable) and seismic data slices (secondary variable). LATEX was used for formatting text, equations, and figures in this work.

1.3 Testing datasets

1.3.1 Blackfoot 3C-3D dataset

The Blackfoot 3C-3D dataset was from the CGG Hampson-Russell software guide dataset and was given to Hampson-Russell from the CREWES project. It was used to implement kriging (in Chapter 2), cokriging (in Chapter 4), and sequential Gaussian simulation using multi-variable cokriging (in Chapter 7). The Blackfoot field, located in southern Alberta, represents a style of stratigraphic trap common in the Western Canadian Basin (Goodway, W. and Tessman, D.J., 2001). The Blackfoot 3C-3D seismic survey was recorded in 1995. The zone of interest is the Mannville Group within the Glauconitic formation.

There were twelve wells involved in this study area, all of which contained calculated porosity logs. The porosity was treated as the primary variable, and was computed an average between the picked top and base of the zone of interest in each well. Figure 1.3 shows the well locations in the survey area and the porosity value at each well location.

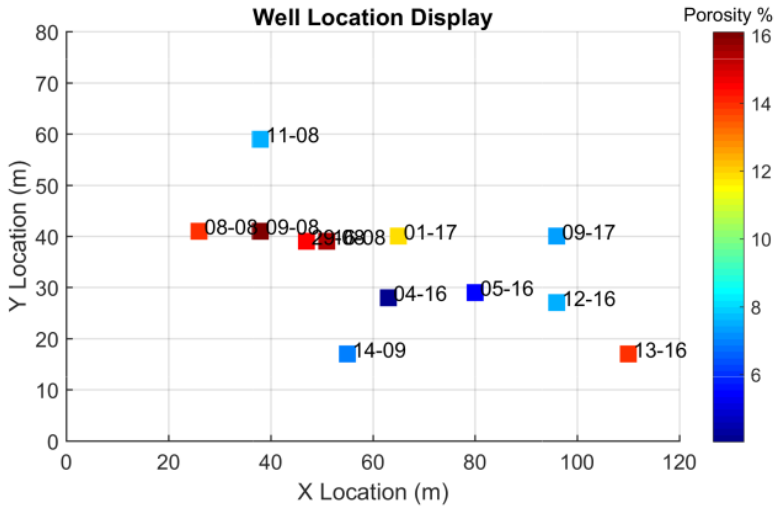

Figure 1.3: Well location display with porosity values

The secondary variable consisted of a data slice extracted from the acoustic impedance inversion of the stacked P-wave seismic data. To obtain the inversion volume, horizons were picked on

the seismic section, an initial model was built from the well logs, and then the model was repeatedly perturbed until the synthetic seismogram for each trace in the volume had the best least-squares match with the original data. Figure 1.4(a) shows crossline 18 from the seismic volume, correlated sonic logs from two intersecting wells, 14-09 and 13-16, and the picked channel top. Figure 1.4(b) shows crossline 18 from the inverted volume. The color key indicates impedance. The data slice of acoustic impedance is displayed in Figure 1.5.

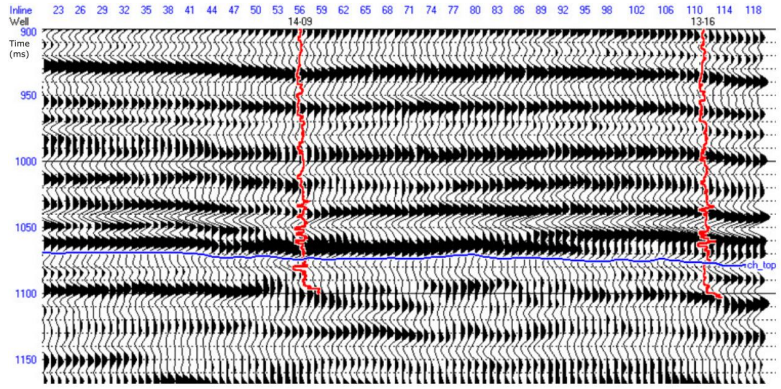

(a) Crossline 18 from the seismic volume

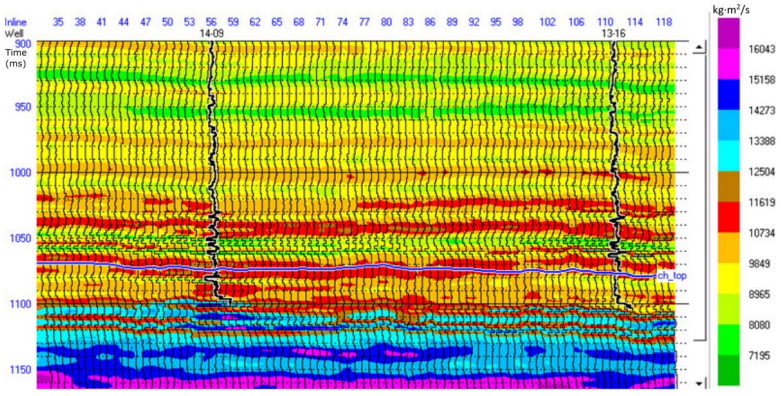

(b) Crossline 18 from the acoustic impedance inverted volume

Figure 1.4: Crossline 18 from the 3D seismic volume

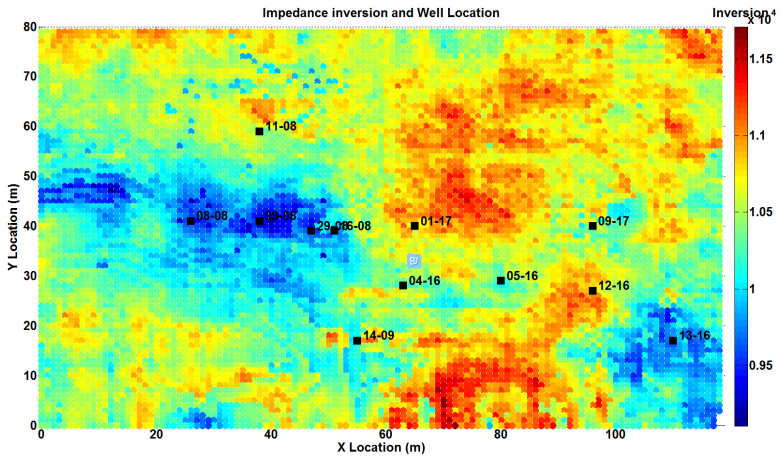

Figure 1.5: Data slice of acoustic impedance inversion

1.3.2 Thickness dataset

The thickness dataset was provided by Murphy Oil Corporation and used for evaluating the performance of cokriging with multiple secondary variables in Chapter 5. The study area is located in northern Alberta and includes 11 drilled wells (Figure 1.6). In this case, the seismic data preconditioning and inversion have been done by CGG GeoConsulting group. A time window from 10 ms above the top reservoir to 10 ms below the base of the non-reservoir clastic was used to produce two seismic attribute slices, seismic amplitude slice and V_p/V_s ratio slice exacted from two volumes shown in Figure 1.7 and Figure 1.8 respectively.

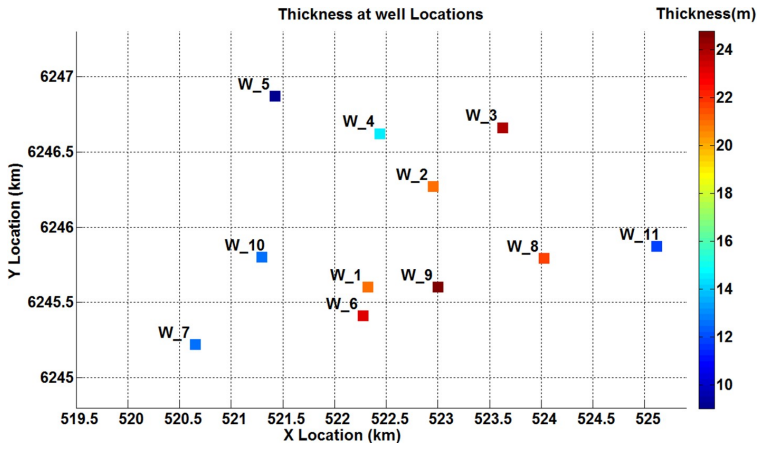

Figure 1.6: Well log distribution and its thickness in study area

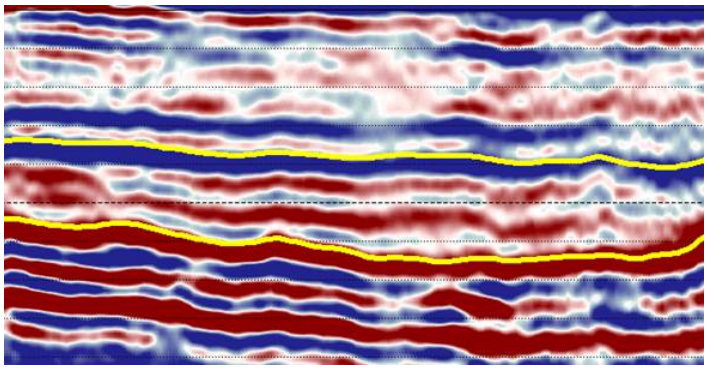

Figure 1.7: Seismic raw amplitude from an angle stack between 8^0 and 29^0

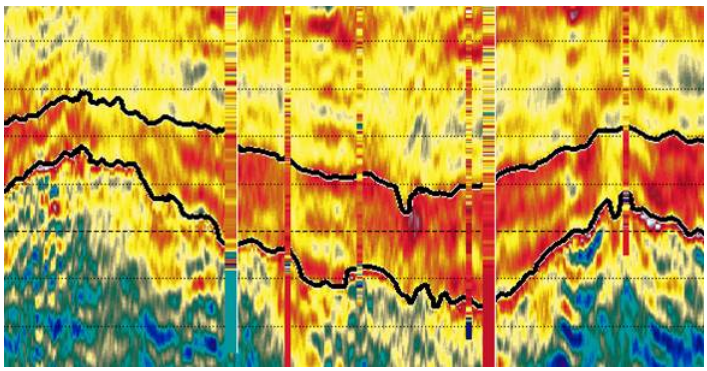

Figure 1.8: Inverted V_p/V_s ratio volume

1.3.3 Total organic carbon dataset

The total organic carbon dataset (TOC) was from a producing shale gas reservoir located in British Columbia, Canada. The number of estimated grid points is over 52,000. Eight drilled wells are distributed in this survey area and shown in Figure 1.9. The value of TOC at each well location is indicated by the color bar. The seismic data volumes were provided by Seitel Canada Ltd. Data cleaning, well-log analysis, well tie, and inversion were completed by CGG GeoConsulting group. A 13 ms window above the base of target zone of interest was used to create two seismic data slices, one is the seismic amplitude shown in Figure 1.10 and another is the V_pV_s ratio in Figure 1.11.

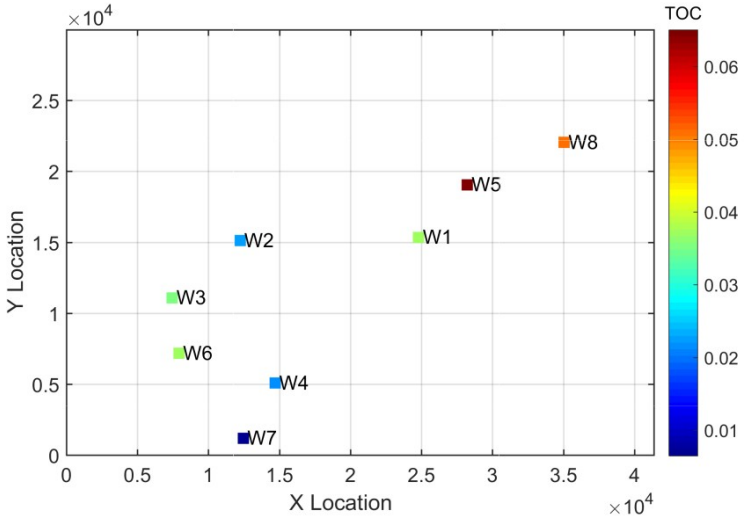

Figure 1.9: Well distribution with TOC values

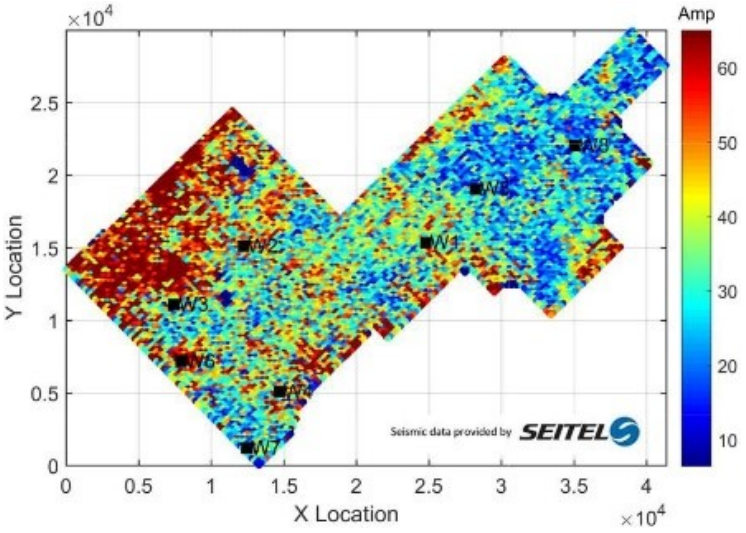

Figure 1.10: Data slice of raw amplitude of an angle stack

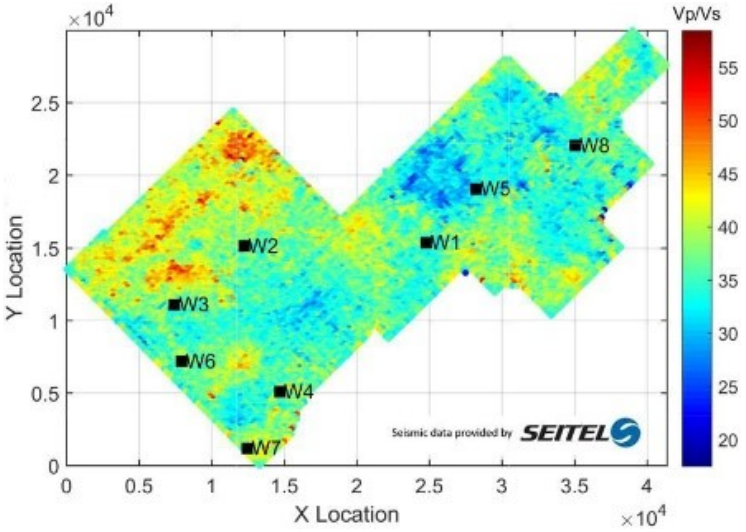

Figure 1.11: Data slice of average V_p/V_s ratio

Chapter 2

Variogram and Kriging

2.1 Variogram

The variogram is a function used to describe the degree of spatial continuity of a dataset. Spatial continuity exists in most earth datasets (Isaaks and Strivastava, 1989). For example, if two data points are closer to each other, their values are more similar than two data points that are farther away.

2.1.1 Introduction to variogram

Wackermagel (2003) presented the theory for all possible well locations, which can be written as

$$2\gamma(\mathbf{h}) = E\left\{[Z(\mathbf{u}) - Z(\mathbf{u}+\mathbf{h})]^2\right\} \tag{2.1}$$

where $\gamma(\mathbf{h})$ is called the **semi-variogram**.

In more practical terms, the variogram for lag distance $\mathbf{h}$ is defined as the average squared difference of values:

$$2\gamma(\mathbf{h}) = \frac{1}{N(\mathbf{h})}\sum[Z(\mathbf{u}) - Z(\mathbf{u}+\mathbf{h})]^2 \tag{2.2}$$

where $N(\mathbf{h})$ is the number of pairs of well values for lag $\mathbf{h}$.

Under the assumption of second-order stationarity, the relationship between the covariance function and semi-variogram is

$$C(\mathbf{0}) = Cov(Z(\mathbf{u},\mathbf{u})) = Var(Z(\mathbf{u})) \tag{2.3}$$

where the covariance with zero lag is equal to the global variance of the variable.

Also, the semi-variogram, with a certain lag **h**, is equal to the difference between the covariance with zero lag and covariance with the same lag.

$$\gamma(\mathbf{h}) = C(\mathbf{0}) - C(\mathbf{h}) \tag{2.4}$$

2.1.2 Characteristics of the semivariogram

As the lag distance between pairs increases, the variability increases, which means the corresponding variogram value will also increase. However, as the lag distance keeps increasing, then the variogram value reaches a plateau. The distance where the variogram reaches this plateau is called the **Range**. When the variogram reaches the range, the plateau is called the **Sill**. The variogram value should be zero when the lag distance is equal to zero. But, in nature, there are several factors, such as measurement errors, that may cause a discontinuity while the lag is equal to zero. The vertical jump from the value of zero at the origin to the value of the variogram is called the **Nugget Effect** (Isaaks and Strivastava, 1989). Nugget, Range, and Sill parameters used to define a spatial variogram are shown in Figure 2.1.

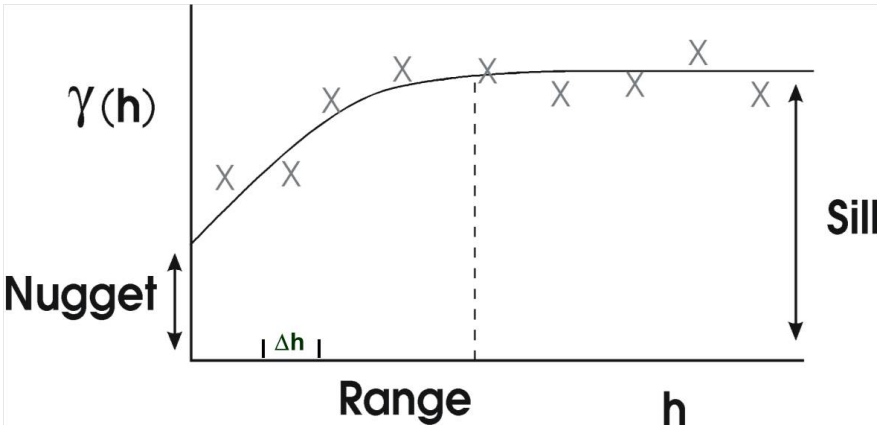

Figure 2.1: The spatial variogram (from Hampson-Russell software guide)

2.1.3 Variogram modelling

The empirical semi-variogram provides spatial information only at certain measured distances, but not all distances. Therefore, it is necessary to fit an empirical semi-variogram. There is no "best" semi-variogram model (Goovaerts, 1997), but here are four most common variogram model types: the Spherical, Exponential, Gaussian, and Nugget variogram models.

Spherical model

Suppose the range of this model is **a**. Then, the semi-variogram and covariance for lag distance **h** are modelled by

$$\gamma(\mathbf{h}) = \begin{cases} 1.5\frac{|\mathbf{h}|}{\mathbf{a}} - 0.5\left(\frac{|\mathbf{h}|}{\mathbf{a}}\right)^3, & \text{if } |\mathbf{h}| < \mathbf{a}; \\ 1, & \textbf{otherwise}. \end{cases} \tag{2.5}$$

$$C(\mathbf{h}) = \begin{cases} 1 - \left(1.5\frac{|\mathbf{h}|}{\mathbf{a}} - 0.5\left(\frac{|\mathbf{h}|}{\mathbf{a}}\right)^3\right), & \text{if } |\mathbf{h}| < \mathbf{a}; \\ 0, & \textbf{otherwise}. \end{cases} \tag{2.6}$$

Exponential model

In the exponential model, **a** is the **practical range** which is the point where $\gamma(|\mathbf{h}| = \mathbf{a})$ is 95% of the **sill** value. The semi-variogram and covariance for lag distance **h** are modelled by

$$\gamma(\mathbf{h}) = 1 - exp\left[-3\frac{|\mathbf{h}|}{\mathbf{a}}\right] \tag{2.7}$$

$$C(\mathbf{h}) = exp\left[-3\frac{|\mathbf{h}|}{\mathbf{a}}\right] \tag{2.8}$$

Gaussian model

In the Gaussian model, **a** is also the **practical range** which is the point where $\gamma(|\mathbf{h}| = \mathbf{a})$ is 95% of the **sill** value. Then, the semi-variogram and covariance for lag distance **h** are modelled by

$$\gamma(\mathbf{h}) = 1 - exp\left[-3\frac{|\mathbf{h}|^2}{\mathbf{a}^2}\right] \tag{2.9}$$

$$C(\mathbf{h}) = exp\left[-3\frac{|\mathbf{h}|^2}{\mathbf{a}^2}\right] \tag{2.10}$$

Nugget model

For the Nugget model, the semi-variogram and covariance introduce a discontinuity at the origin

$$\gamma(\mathbf{h}) = \begin{cases} 0, & \text{if } |\,\mathbf{h}\,| = 0; \\ 1, & \textbf{otherwise}. \end{cases} \tag{2.11}$$

$$C(\mathbf{h}) = \begin{cases} 1, & \text{if } |\,\mathbf{h}\,| = 0; \\ 0, & \textbf{otherwise}. \end{cases} \tag{2.12}$$

2.2 Kriging

Kriging is an interpolation technique using only sparsely sampled data points. It is different from the Inverse Distance Weighting (IDW) method because the kriging weights not only rely on the distance between the estimate point and the observed point, but also are correlated with the spatial distribution based on the semi-variogram. A semi-variogram model defines the spatial relationship between all the sample data points.

2.2.1 Introduction to kriging

Kriging is often associated with the acronym **BLUE** (Best, Linear, Unbiased, Estimation) where:

Best: This method is "best" because it minimizes the variance of the errors.

Linear: The final estimates are weighted linear combinations of the input samples.

Unbiased: The mean residual or error is equal to 0.

Estimate: The final result is a prediction.

In mathematics, the estimate point in kriging can be calculated as

$$a_0 = \omega_1 a_1 + \omega_2 a_2 + \omega_3 a_3 + \omega_4 a_4 + \cdots \tag{2.13}$$

where a_0 is an estimate, ω_i is the corresponding weight of the i^{th} observed value, a_i.

In order to compute the estimated value a_0 in Eq. 2.13, a vector of weights $(\omega_1, \omega_2, ...\omega_n)$ is the only parameter required to be calculated since the observed samples $(a_1, a_2, ...a_n)$ are known points. The vector of weights can be written as

$$\mathbf{C}\,\mathbf{w} = \mathbf{d} \tag{2.14}$$

where C is the covariance matrix of the known points, w is a vector containing the corresponding weights, and d is the covariance vector between the estimate point and known points.

Eq. 2.14 can be rewritten as

$$\mathbf{w} = \mathbf{C}^{-1}\,\mathbf{d} \tag{2.15}$$

Examples of the covariance matrix C and weight covariance vector are given in the next section.

2.2.2 Simple kriging and ordinary kriging

(1) **Simple kriging**

For simple kriging, the mean is assumed to be the same in the entire estimate domain. In other words, assume the constant, known mean $m(\mathbf{u})$ is equal to m , $(m(\mathbf{u}) = m)$, so that

$$Z_{SK}(\mathbf{u}) = m + \Sigma\lambda_a(\mathbf{u})\,[Z(\mathbf{u}_a) - m] \tag{2.16}$$

This estimate (Eq. 2.16) is automatically unbiased because we assume $E\,[Z(\mathbf{u}) - m] = 0$. Therefore, $E\,[Z_{SK}(\mathbf{u})] = m = E\,[Z(\mathbf{u})]$.

The corresponding weights in the simple kriging method can be written as a matrix form as

$$\begin{pmatrix} C_{11} & C_{12} & C_{13} & \cdots & C_{1n} \\ C_{21} & C_{22} & C_{23} & \cdots & C_{2n} \\ C_{31} & C_{32} & C_{33} & \cdots & C_{3n} \\ \vdots & \vdots & \vdots & \ddots & \vdots \\ C_{n1} & C_{n2} & C_{n3} & \cdots & C_{nn} \end{pmatrix} \begin{pmatrix} \omega_1 \\ \omega_2 \\ \omega_3 \\ \vdots \\ \omega_n \end{pmatrix} = \begin{pmatrix} C_{10} \\ C_{20} \\ C_{30} \\ \vdots \\ C_{n0} \end{pmatrix} \tag{2.17}$$

where C_{ij} is the covariance between two points i and j; ω_i is the kriging weight of the i^{th} measurement point.

To compute the vector of weights of simple kriging, Eq. 2.17 can be rewritten as

$$\begin{pmatrix} \omega_1 \\ \omega_2 \\ \omega_3 \\ \vdots \\ \omega_n \end{pmatrix} = \begin{pmatrix} C_{11} & C_{12} & C_{13} & \cdots & C_{1n} \\ C_{21} & C_{22} & C_{23} & \cdots & C_{2n} \\ C_{31} & C_{32} & C_{33} & \cdots & C_{3n} \\ \vdots & \vdots & \vdots & \ddots & \vdots \\ C_{n1} & C_{n2} & C_{n3} & \cdots & C_{nn} \end{pmatrix}^{-1} \begin{pmatrix} C_{10} \\ C_{20} \\ C_{30} \\ \vdots \\ C_{n0} \end{pmatrix} \tag{2.18}$$

Consider a simple kriging example with two sample points (Figure 2.2). Suppose there are two known points a_1 and a_2, and a_0 is the point to be predicted.

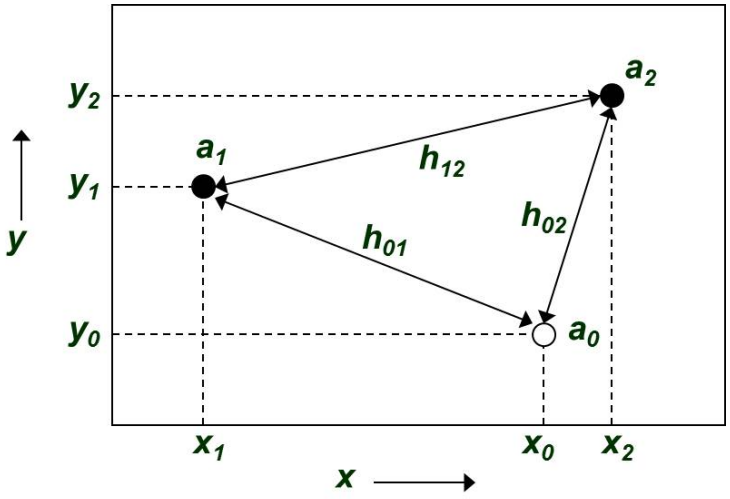

Figure 2.2: Simple kriging with two points (from Hampson-Russell software user guide)

The corresponding weights of the simple kriging technique can be written as

$$\begin{pmatrix} \omega_1 \\ \omega_2 \end{pmatrix} = \begin{pmatrix} C_0 & C(h_{12}) \\ C(h_{12}) & C_0 \end{pmatrix}^{-1} \begin{pmatrix} C(h_{01}) \\ C(h_{02}) \end{pmatrix} \tag{2.19}$$

(2) **Ordinary kriging**

For ordinary kriging, we assume that there is a local mean around each predicated point instead of

a constant mean in the whole estimate area. This means $m(\mathbf{u}_a) = m(\mathbf{u})$ for each nearby data. The function of ordinary kriging can be written as

$$\begin{aligned} Z_{OK}(\mathbf{u}) &= m(\mathbf{u}) + \sum \lambda_a(\mathbf{u}) \left[Z(\mathbf{u}_a) - m(\mathbf{u}) \right] \\ &= \sum \lambda_a(\mathbf{u}) Z(\mathbf{u}_a) + \left[1 - \sum \lambda_a(\mathbf{u}) \right] m(\mathbf{u}) \end{aligned} \tag{2.20}$$

To remove the unknown local mean, $m(\mathbf{u})$, we set the sum of the kriging weights ($\sum \lambda_a(\mathbf{u})$) equal 1. Thus, the function of ordinary kriging can be rewritten as

$$Z_{OK}(\mathbf{u}) = \sum \lambda_a(\mathbf{u}) Z(\mathbf{u}_a) \tag{2.21}$$

where $\sum \lambda_a(\mathbf{u}) = 1$.

The corresponding weights of ordinary kriging can then be defined in the matrix form as

$$\begin{pmatrix} C_{11} & C_{12} & C_{13} & \cdots & C_{1n} & 1 \\ C_{21} & C_{22} & C_{23} & \cdots & C_{2n} & 1 \\ C_{31} & C_{32} & C_{33} & \cdots & C_{3n} & 1 \\ \vdots & \vdots & \vdots & \ddots & \vdots & \vdots \\ C_{n1} & C_{n2} & C_{n3} & \cdots & C_{nn} & 1 \\ 1 & 1 & 1 & \cdots & 1 & 0 \end{pmatrix} \begin{pmatrix} \omega_1 \\ \omega_2 \\ \omega_3 \\ \vdots \\ \omega_n \\ \mu \end{pmatrix} = \begin{pmatrix} C_{10} \\ C_{20} \\ C_{30} \\ \vdots \\ C_{n0} \\ 1 \end{pmatrix} \tag{2.22}$$

where C_{ij} is the covariance between two points i and j; ω_i is kriging weight of the i^{th} measurement point; μ is the Lagrange parameter.

To compute the vector of weights of ordinary kriging, Eq. 2.22 can be rewritten as

$$\begin{pmatrix} \omega_1 \\ \omega_2 \\ \omega_3 \\ \vdots \\ \omega_n \\ \mu \end{pmatrix} = \begin{pmatrix} C_{11} & C_{12} & C_{13} & \cdots & C_{1n} & 1 \\ C_{21} & C_{22} & C_{23} & \cdots & C_{2n} & 1 \\ C_{31} & C_{32} & C_{33} & \cdots & C_{3n} & 1 \\ \vdots & \vdots & \vdots & \ddots & \vdots & \vdots \\ C_{n1} & C_{n2} & C_{n3} & \cdots & C_{nn} & 1 \\ 1 & 1 & 1 & \cdots & 1 & 0 \end{pmatrix}^{-1} \begin{pmatrix} C_{10} \\ C_{20} \\ C_{30} \\ \vdots \\ C_{n0} \\ 1 \end{pmatrix} \tag{2.23}$$

2.3 Case study

In the kriging family, ordinary kriging is very popular because the semi-variogram exhibits the local stationarity (Gonzalez, J., 2013). In this study, the ordinary kriging method will be applied to the Blackfoot 3C-3D dataset to predict porosity. Porosity estimation plays an important role in geoscience since it is an essential key in predicting reservoir and elastic rock properties. Many techniques and algorithms have been introduced to predict porosity in subsurface reservoirs, for instance, kriging. The kriging work-flow designed is shown in Figure 2.3.

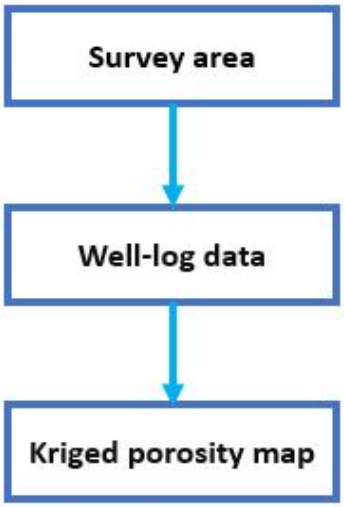

Figure 2.3: Kriging work-flow

The well distribution with porosity values is displayed in Figure 2.4 where the color bar indicates the porosity value. To compute the ordinary kriging weights, an auto-variogram based on the sampled porosity data has been constructed and is shown in Figure 2.5. The final kriged porosity map is displayed in Figure 2.6.

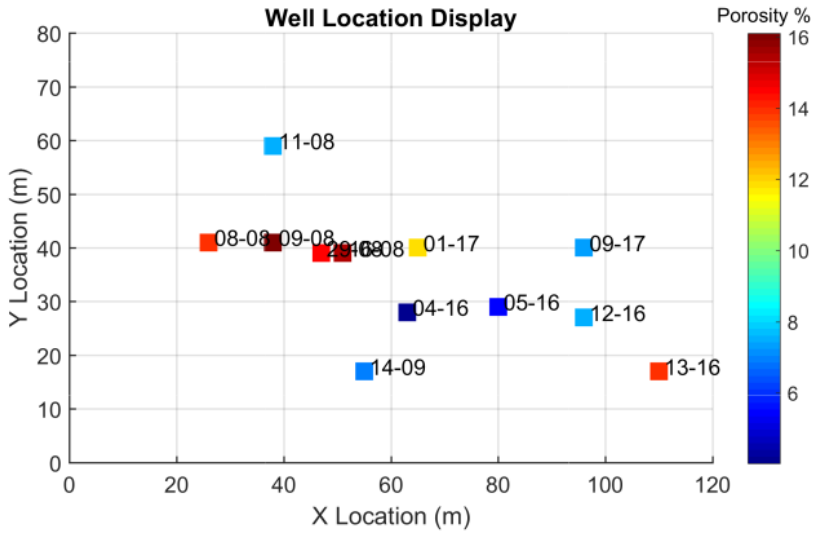

Figure 2.4: Well location display with porosity values

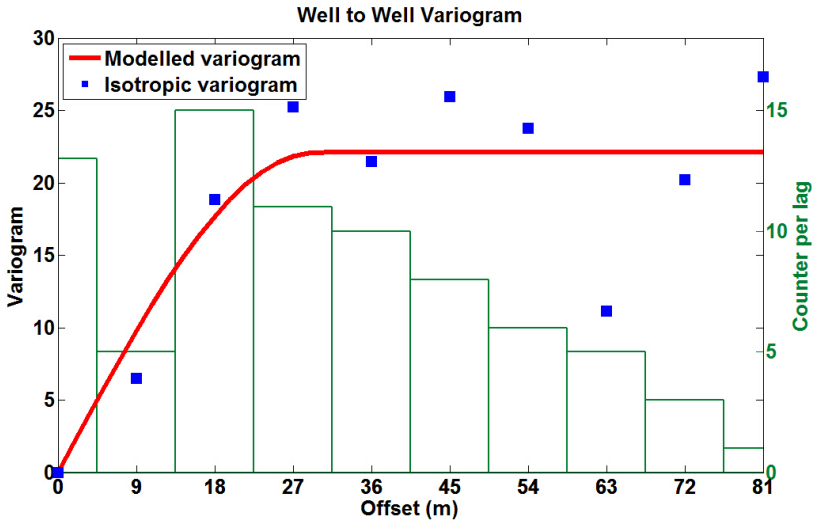

Figure 2.5: Well to well variogram

Compared to the well distribution map with porosity values (Figure 2.4), the interpolated result (Figure 2.6) generated by kriging illustrates the main trend of the porosity distribution but is overly

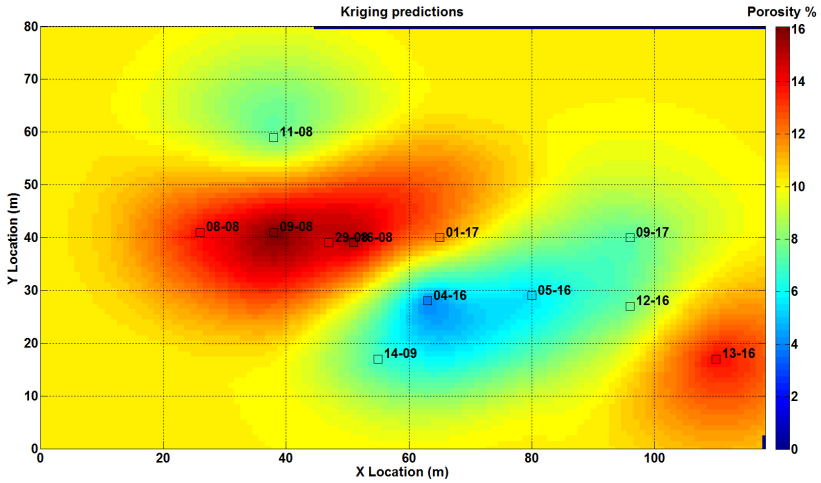

Figure 2.6: Kriging interpolation with porosity

smooth. From the produced map, the "bulls-eyes" effect around the well intersections can be observed. It occurs because the ordinary kriging method averages the values between sample data points.

2.4 Conclusions

In this chapter, the kriging method was introduced and applied to the Blackfoot 3C-3D dataset to generate a porosity map. There are three advantages of kriging. (1) The kriging weights are more accurate than other mapping methods because they are calculated based on the semi-variogram that captures the spatial relationship between sample data points. (2) The kriging method is easy to use. Only the primary data and its semi-variogram are required during the process. (3) The kriging method honours the well-log data (the primary data) at all the well locations. However, two disadvantages can be observed as well. (1) The predicted porosity values appear as being too smooth. (2) The kriged map shows a "bulls-eyes" effect.

Chapter 3

Cross validation

3.1 Introduction

Cross-validation is a testing method used to measure the predictive performance of an estimated model. In other words, cross-validation is used to evaluate how well the model can generalize to an independent dataset (Isaaks and Strivastava, 1989). In a prediction problem, over-fitting an estimated model may not work well. For instance, if we keep adding higher order terms to make the data fit better, then after applying this model to a new dataset, the prediction could get worse as the higher order terms are added, since the over-fitting can fit noisy samples too well. Cross-validation can be used to prevent over-fitting. Additionally, it allows us to compare the predicted value and the true value using only the information available in the sample dataset.

3.2 Classification

3.2.1 Non-exhaustive cross-validation

The non-exhaustive cross-validation method will not compute all the combinations for separating the sample points. In this section, two methods, **Holdout** and **K-fold**, are introduced.

(1) Holdout method

The holdout method requires two datasets. One is called the training dataset and another is called the validation dataset. The training dataset is fitted to the model. The validation dataset is used to evaluate the model. After multiple runs, the errors between the true values and the corresponding predicted values are accumulated as an indicator to evaluate the model. The disadvantage of this method is that the evaluation results may be highly different depending on which data

points are assigned to the training set and which data points are assigned to the validation set. ($www.cs.cmu.edu/\ schneide/tut5/node42.html$)

(2) K-fold method

In K-fold cross-validation, the dataset is randomly divided into **K** equally sized sub-datasets. Each sub-dataset is not only used as the validation dataset for evaluating the model, but also as the training dataset. The validation process has to be repeated **K** times. In each time during the process, one of **K** sub-datasets is used as the validation dataset only once. The errors from each process will be averaged as the final evaluation result. The advantage of this method is that all sample points are used for both training and validation.

3.2.2 Exhaustive cross-validation

The exhaustive cross-validation method involves dividing the data into all possible combinations of training and validation datasets.

(1) Leave-one-out cross-validation

Leave-one-out cross-validation calculates the difference between the predicted value and the actual value by removing one sample point at a time and computing the root-mean-square (**RMS**) error each time. The accuracy measures are described as below and displayed in Figure 3.1.
Suppose there are n independent sample points $Z(x_1), Z(x_2), ...Z(x_n)$.

(1) Let the sample point $Z(x_i)$ be the test data. Then, fit the model by the rest of the sample points. The error between the true value and the predicted value is computed.

(2) Repeat **n** times, so that all the sample points are treated as a test data exactly once.

(3) Compute the average error of leaving each point out and express as

$$\mathbf{E_{RMS}} = \sqrt{\frac{1}{N}\sum_{i=1}^{N}\left\{z(x_i) - \hat{z}(x_i)\right\}^2} \tag{3.1}$$

where $z(x_i)$ is the actual value and $\hat{z}(x_i)$ is the estimated value by leaving one out.

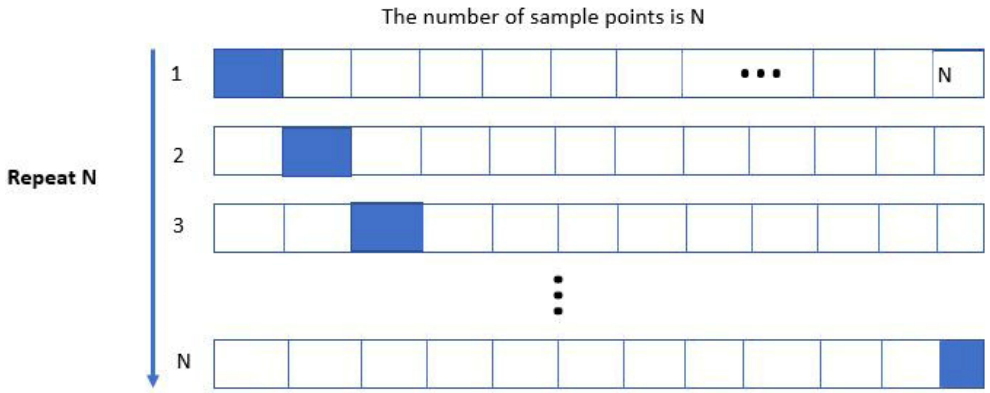

Figure 3.1: Leave-one-out cross-validation

In Figure 3.1, the blue point is a test data and all the rest of white points are treated as training data in each time.

In the following of chapters, the leave-one-out cross-validation will be used to evaluate cokriging (in Chapter 4) and cokriging with multiple secondary attributes (in Chapter 5).

Chapter 4

Cokriging

4.1 Introduction

Geostatistical methods, such as cokriging, can be applied to integrate well-log data and seismic data to improve the lateral resolution of the final results. Cokriging, an extension of kriging, has been employed in porosity prediction since it was introduced into the geophysical industry by Doyen (1988) based on the theory developed by Matheron (1965). The objective of the cokriging technique is to use attributes, such as acoustic impedance, amplitude or travel time extracted from 3D seismic data, as a secondary variable to guide the interpolation of related well log data, which is referred to as the primary variable, such as porosity, shale volume or depth. The primary variables are usually sparsely sampled, but the secondary variables are densely sampled over the survey area and are assumed to be closely correlated with the primary variable (Figure 4.1).

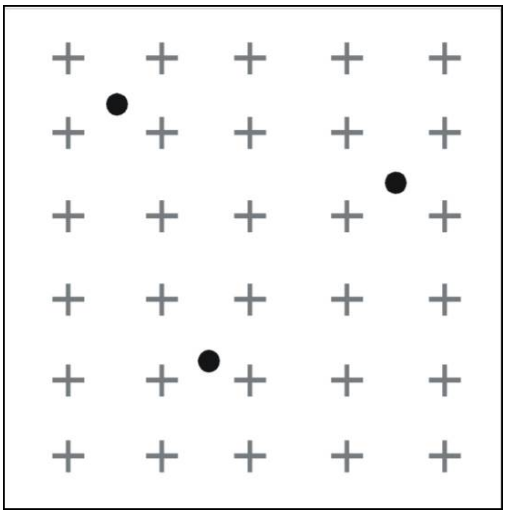

Figure 4.1: Distribution of primary and secondary variables, where primary variables are shown as • symbols and secondary variables as + signs.

In Figure 4.1, the symbol + represents the seismic data (secondary variable), which are dense, but with poor vertical resolution; the symbol • represents the well-log data (primary variable), which are sparse, but with good vertical resolution.

Secondary variables bring useful information related to the primary variable (Isaaks and Strivastava, 1989). Doyen (1988) applied cokriging to predict porosity by acoustic impedance, extracted from 3D seismic data, as the secondary variable. Cokriging produces maps that contain trends constructed by the spatial correlation function to model the lateral variations of the reservoir properties (Doyen et al.,1996).

4.2 Ordinary cokriging

The cokriging function is a linear combination of primary and secondary variables as

$$u_0 = \sum_{i=1}^{n} a_i u_i + \sum_{j=1}^{m} b_j v_j \tag{4.1}$$

where u_0 is the estimate at location 0; u_i is the primary variable and the number of the primary variables at the nearby locations is n where $i = 1,\ldots,n$; v_j is the secondary variable and the number of the secondary variables at the nearby locations is m where $j = 1,\ldots,m$; a_i and b_j are the corresponding weights of primary and secondary variables.

To satisfy the unbiasedness condition, the expected value of the estimate can be written as

$$\begin{aligned} E\{u_0\} &= E\{\textstyle\sum_{i=1}^{n} a_i u_i + \sum_{j=1}^{m} b_j v_j\} \\ &= \textstyle\sum_{i=1}^{n} a_i E\{u_i\} + \sum_{j=1}^{m} b_j E\{v_j\} \\ &= m_u \textstyle\sum_{i=1}^{n} a_i + m_v \sum_{j=1}^{m} b_j \end{aligned} \tag{4.2}$$

where $E\{u_i\} = m_u$ and $E\{v_i\} = m_v$.

Thus, the sum of primary weights is required to be 1 and the sum of secondary weights is required to be 0.

Then, matrix form of the cokriging weights can be written as

$$\begin{pmatrix} C_{uu} & C_{uv} & \mathbf{1} & \mathbf{0} \\ C_{vu} & C_{vv} & \mathbf{0} & \mathbf{1} \\ \mathbf{1}^T & \mathbf{0} & 0 & 0 \\ \mathbf{0} & \mathbf{1}^T & 0 & 0 \end{pmatrix} \begin{pmatrix} \mathbf{a} \\ \mathbf{b} \\ -\mu_1 \\ -\mu_2 \end{pmatrix} = \begin{pmatrix} C_{u_0 u} \\ C_{u_0 v} \\ 1 \\ 0 \end{pmatrix} \tag{4.3}$$

where **a** is a vector of primary variable weights, **b** is a vector of secondary variable weights,

μ_1 and μ_2 are the Lagrange parameters,

$C_{uu} = Cov(u_i, u_j)$ is the auto-covariance of the primary variables,

$C_{vv} = Cov(v_i, v_j)$ is the auto-covariance of the secondary variables, and

$C_{uv} = Cov(v_i, v_j)$ is the cross-covariance between the primary and secondary variables,

Additionally, the cokriging matrix is symmetric, which means that $C_{uv} = C_{vu}$

To compute the vector of primary variable weights and the vector of secondary variable weights, Eq. 4.3 can be rewritten as

$$\begin{pmatrix} \mathbf{a} \\ \mathbf{b} \\ -\mu_1 \\ -\mu_2 \end{pmatrix} = \begin{pmatrix} C_{uu} & C_{uv} & \mathbf{1} & \mathbf{0} \\ C_{vu} & C_{vv} & \mathbf{0} & \mathbf{1} \\ \mathbf{1}^T & \mathbf{0} & 0 & 0 \\ \mathbf{0} & \mathbf{1}^T & 0 & 0 \end{pmatrix}^{-1} \begin{pmatrix} C_{u_0 u} \\ C_{u_0 v} \\ 1 \\ 0 \end{pmatrix} \tag{4.4}$$

In ordinary cokriging, we assume that the sum of the weights of the primary variable is equal to one and the sum of the weights of the secondary variable is equal to zero. A problem may arise because the sum of the weights of the secondary variable is equal to zero. If some of the secondary variable weights are positive, then the others must be negative. It is highly possible that the final predicted results might be negative. To avoid this situation, standardized ordinary cokriging is introduced in the next.

4.3 Standardized ordinary cokriging

For standardized ordinary cokriging, we can adjust the secondary variable such that the mean of secondary variable can be treated the same as the mean of primary variable. The function of standardized ordinary cokriging can be written as

$$u_0 = \sum_{i=1}^{n} a_i u_i + \sum_{j=1}^{m} b_j (v_j - m_v + m_u) \tag{4.5}$$

$$\sum_{i=1}^{n} a_i + \sum_{j=1}^{m} b_j = 1 \tag{4.6}$$

where m_u is the estimated mean of the primary variable and m_v is the estimated mean of the secondary variable.

4.3.1 Case study

In this case study, the Blackfoot 3C-3D dataset is used to create a porosity map by the ordinary cokriging method. In oil and gas exploration, porosity can be one of best indicators of hydrocarbon reservoir, since it indicates the amount of pore space in the reservoir that may contain hydrocarbon. By combining the well-log data and seismic attribute, porosity prediction by cokriging can be more accurate than by kriging. The cokriging work-flow is displayed in Figure 4.2.

Twelve wells containing calculated porosity logs (the primary variable) are distributed over the survey area and displayed in Figure 4.3 where the color bar indicates the value of porosity. To create the secondary variable, three seismic slices, seismic amplitude, amplitude envelope, and instantaneous phase, were computed from the survey using a 10 ms RMS average below the picked channel top from the stacked P-wave seismic volume. Similarly, one more seismic slice was extracted from the model-based acoustic impedance inversion using an arithmetic average in a 10 ms window over the zone of interest.

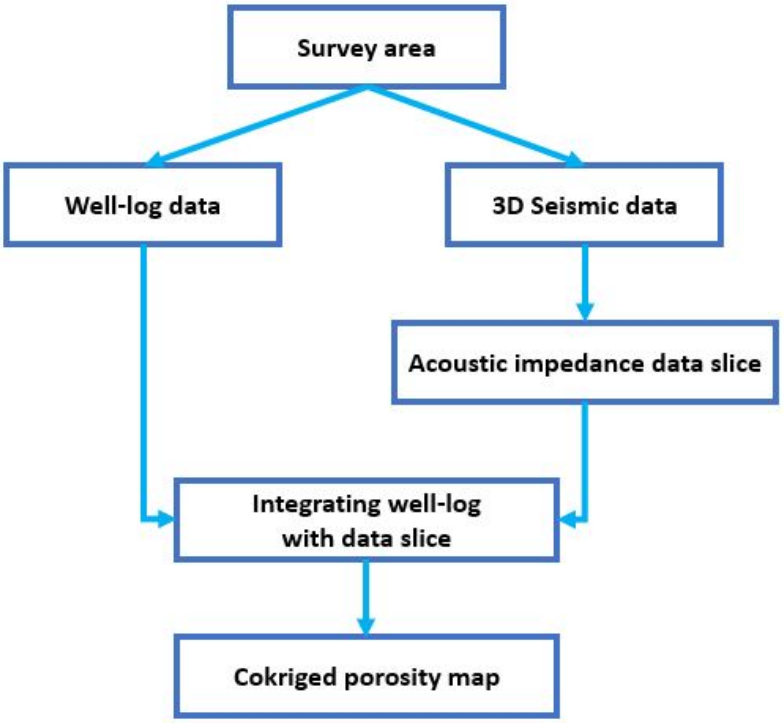

Figure 4.2: The cokriging work-flow

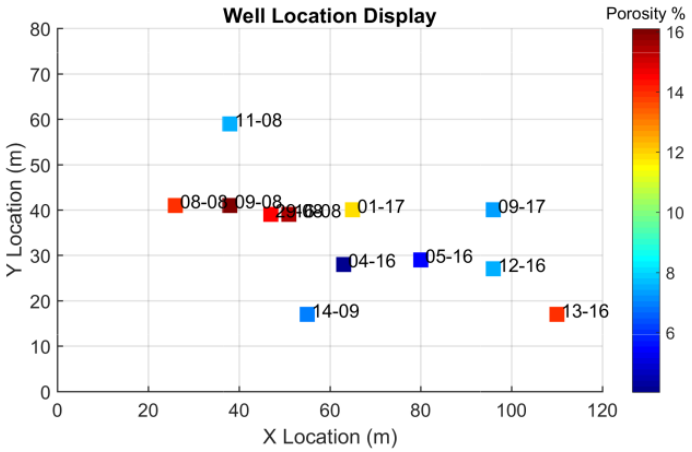

Figure 4.3: Well location display with porosity values

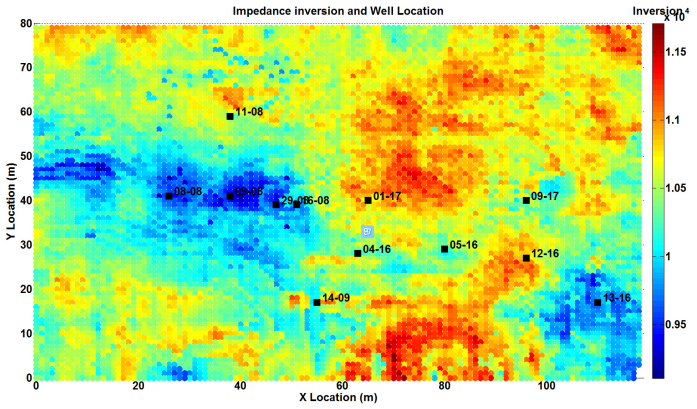

Figure 4.4: Data slice of acoustic impedance inversion

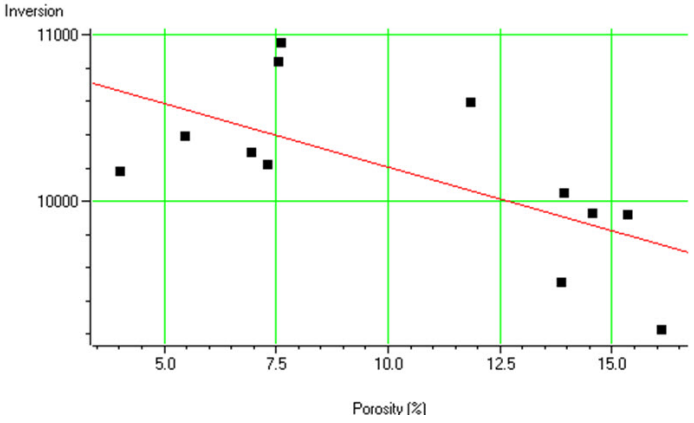

Figure 4.5: Cross-plot between porosity and data slice of acoustic impedance

The cokriging estimation system works best when there is a strong correlation between the primary and secondary variables. Thus, we calculated correlation coefficients between the porosity values and all four seismic slices. The acoustic impedance slice displayed in Figure 4.4 was picked as the secondary variable because it showed the highest correlation (-0.65) with porosity. The cross-plot between porosity and acoustic impedance data slice is displayed in Figure 4.5.

To compute the cokriging weights, auto-semi-variograms of porosity and aoustic impedance data slice are computed as well as the cross-semi-variogram between porosity and acoustic impedance data slice. All the semi-variograms are displayed in Figure 4.6. Utilizing the primary and secondary datasets to implement Eq. (4.4) to compute the cokriging weights, the final cokriged poros-

ity map has been created and shown in Figure 4.7.

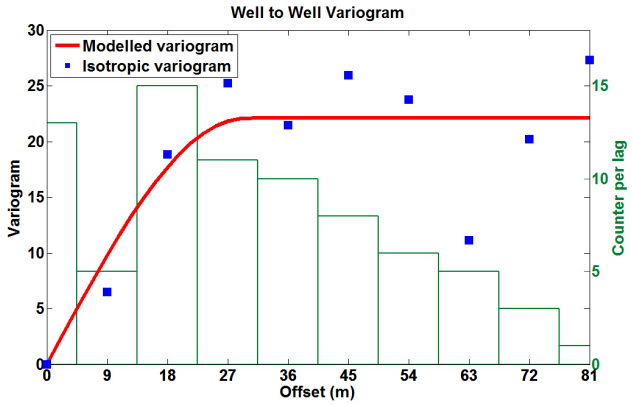

(a) Well to well variogram

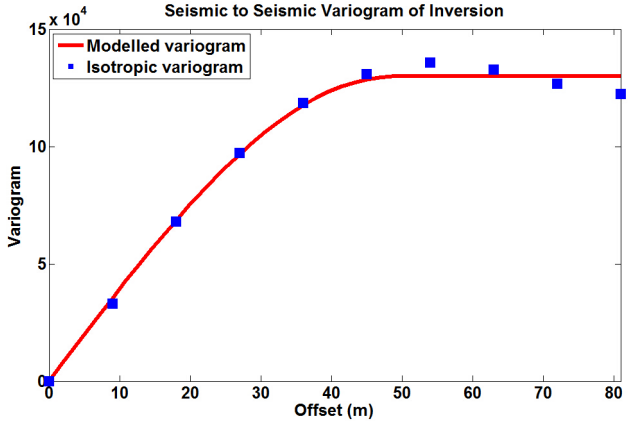

(b) Seismic to seismic variogram

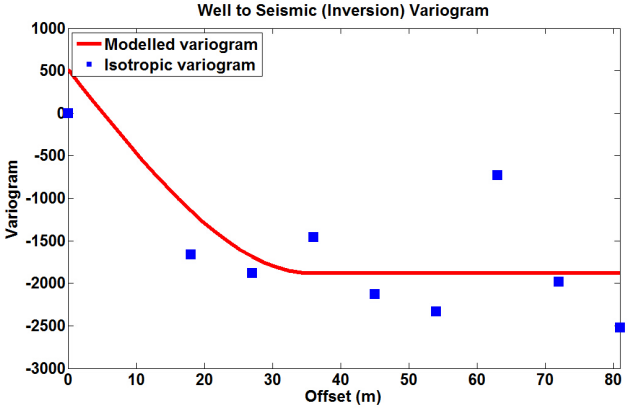

(c) Well to seismic variogram

Figure 4.6: Variograms

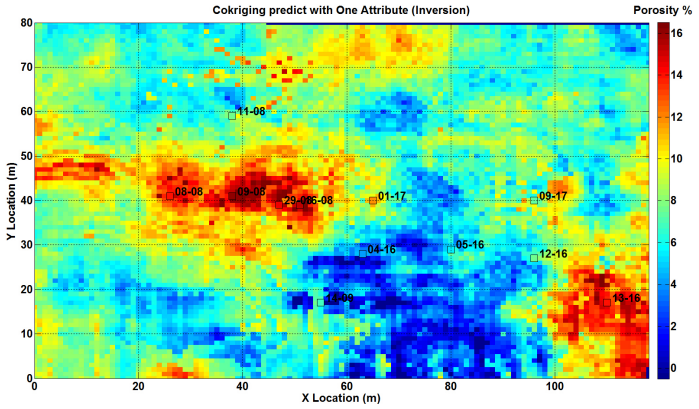

Figure 4.7: Cokriging with porosity and inversion slice

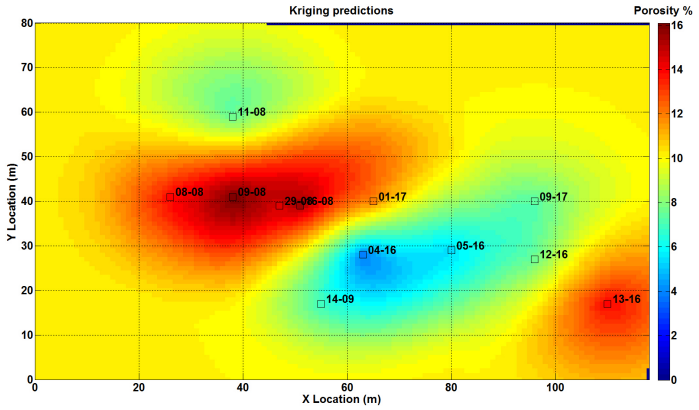

Figure 4.8: Kriging with porosity only

Compared to the well distribution map (Figure 4.3), both the cokriged porosity map (Figure 4.7) and kriged porosity map (Figure 4.8) delineate the major trend. However, the lateral resolution has been improved in the cokriged version through the introduction of a seismic attribute as the secondary variable. Leave-one-out cross-validation was applied to validate the accuracy of the cokriging and kriging results. The cokriging system shows a lower RMS error than the RMS error of kriging in Figure 4.9.

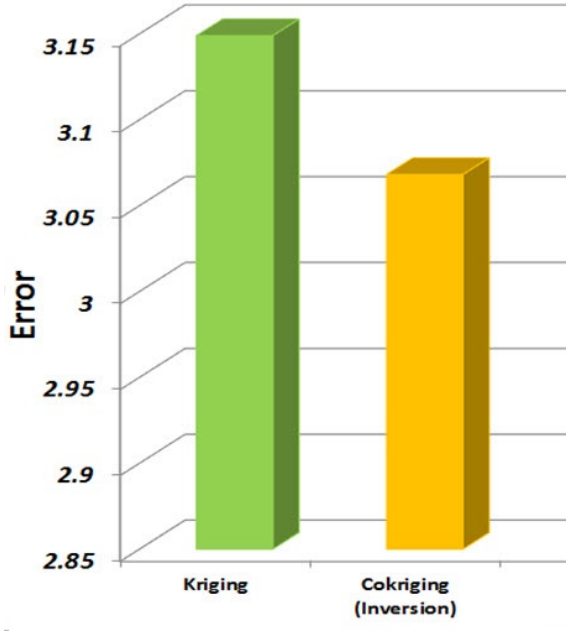

Figure 4.9: Leave-one-out cross validation

4.3.2 Conclusions

In this chapter, the cokriging system with a secondary variable has been implemented. The case study showed that both the kriging and cokriging methods honor to the well-log data and are able to display the major trend. Compared to kriging, cokriging has additional advantages. A secondary variable with useful geological information related to the primary data can enhance the final interpretation map. In general, the primary variable has been laterally sampled sparsely, but the secondary variable has been laterally sampled densely, which can help to estimate the primary variable at unsampled locations. In the case study, the cokriged porosity map showed a significant improvement in lateral definition of porosity due to the geological information introduced. Cokriging can reduce the likelihood of dependency problems caused using an imprecise primary semi-variogram only. Additionally, leave-one-out cross-validation has been applied to both kriging and cokrigng, the cokriging estimate variance is lower than the kriging's estimate.

Chapter 5

Cokriging with multiple secondary variables

5.1 Introduction

Lithologic reservoir characterization using a combination of well-log data and seismic attributes has improved as more advanced techniques of seismic exploration and analysis have been developed. In the traditional cokriging system, only a single secondary variable is allowed in calculation. It is beneficial to use more than one seismic attribute to support the prediction because each attribute may have unique information about the reservoir rock properties (Guerrero et al., 1996). Elastic parameters derived from seismic data can be utilized as distinct indicators to discriminate the properties of oil and gas reservoirs. For instance, inverted elastic parameters and the AVO gradient and intercept often reveal the fluid content of the reservoir (Castagna and Smith, 1994, Li and Chen, 2008). Elastic impedance and V_p/V_s ratio extracted from prestack inversion are good indicators to identify the thickness and lithology of the reservoir (Connolly, 1999, Duffaut et al., 2000, Dumitrescu and Lines, 2006). Acoustic impedance and amplitude from post-stack seismic data will also highlight the gas/oil potential of a reservoir, and can also be implemented to estimate the sand thickness (Marfurt and Kirlin, 2001).

To optimize the secondary data, numerous methods have been proposed. Russell et al. (2002) combined cokriging and multi-attribute transforms. As Russell et al. (2002) illustrated, the secondary variable of cokriging is an improved map generated by multi-attribute analysis. A limitation of this method is that the multi-attribute algorithm assumes that the predicted area are highly correlated to the well tie locations. Babak and Deutsch (2009) improved the cokriging model by merging all secondary variables into a single super-secondary variable. However, this super-secondary data was obtained under assumptions which are unpractical. For example, the linear combination of all secondary data is assumed to generate the super data by merging all these secondary data.

In this chapter, an approach to introduce more than one secondary variable in the cokriging system is presented. This method reduces prior assumptions and improve the estimation. This also means that more than one seismic attribute or elastic parameter can be integrated into the cokriging approach. Three criteria should be considered in the secondary attribute selection for improved cokriging: 1) The attributes should be highly correlated with expected goals i.e., the properties of the reservoir derived from well logs; 2) The attributes should be sensitive to reservoir properties and represent different lithologies; 3) The attributes should be independent or weakly dependent. As an evaluation of the improved cokriging approach, the method is applied to estimate the thickness and distribution of a lithologic reservoir.

5.2 Methodology

By modifying the derivation of rescaled ordinary cokriging (ROCK) (Goovaerts, 1998), I will demonstrate how to derive an improved cokriging system involving more than one secondary variable. The reason for using ROCK is in considering the unique variation in magnitude of the seismic attributes, which can reduce the uncertainty. One single constraint for cokriging weights may decrease the risk of reaching at unacceptable negative concentrations and enhance the role of secondary information (Goovaerts, 1998).

Taking the improved ROCK method involving two secondary variables as an example, the estimator $\hat{u}_0$ of the improved ROCK method with two secondary variables at location 0 is defined as

$$\hat{u}_0 = \sum_{i=1}^{n} a_i u_i + \sum_{j=1}^{m} b_j (v_j - \widetilde{m}_v + \widetilde{m}_u) + \sum_{k=1}^{p} c_k (x_k - \widetilde{m}_x + \widetilde{m}_u) \tag{5.1}$$

where u_1, u_2, ... , u_n are the primary data at n locations; v_1, v_2, ... , v_m and x_1,x_2, ... , x_p are the secondary data at **m** locations and **p** locations. a_1,a_2, ... , a_n, b_1,b_2, ... , b_m, and c_1, c_2, ... , c_p are cokriging weights to be determined. $\widetilde{m}_u$, $\widetilde{m}_v$, and $\widetilde{m}_x$ are means of primary, first secondary, and second secondary variables, respectively.

One single constraint for weights can be achieved for the estimator in Eq. (5.1), which can be expressed as

$$\sum_{i=1}^{n} a_i + \sum_{j=1}^{m} b_i + \sum_{k=1}^{p} c_k = 1 \tag{5.2}$$

Then, the estimation error can be written as

$$\mathbf{R} = \hat{u}_0 - u_0 = \mathbf{w^t Z} \tag{5.3}$$

where $\mathbf{w^t}$ = (a_1, a_2, …, a_n, b_1,b_2, … , b_m, c_1, c_2, … , c_p, -1) and $\mathbf{Z^t}$ = (u_1, u_2, … , u_n, v_1, v_2, … , v_m, x_1,x_2, … , x_p, $\mathbf{u_0}$).

Therefore, the variance of $\mathbf{R}$ can be expressed as

$$\begin{aligned}
\mathbf{Var}\{\mathbf{R}\} &= \mathbf{w^t C_z w} \\
&= \sum_{i=1}^{n}\sum_{j=1}^{n} a_i a_j Cov\{u_i u_j\} + \sum_{i=1}^{m}\sum_{j=1}^{m} b_i b_j Cov\{v_i v_j\} + \sum_{i=1}^{p}\sum_{j=1}^{p} c_i c_j Cov\{x_i x_j\} \\
&+ 2\sum_{i=1}^{n}\sum_{j=1}^{m} a_i b_j Cov\{u_i v_j\} + 2\sum_{i=1}^{n}\sum_{j=1}^{p} a_i c_j Cov\{u_i x_j\} + 2\sum_{i=1}^{m}\sum_{j=1}^{p} b_i c_j Cov\{v_i x_j\} \\
&- 2\sum_{i=1}^{n} a_i Cov\{u_i u_0\} - 2\sum_{i=1}^{m} b_i Cov\{v_i u_0\} - 2\sum_{i=1}^{p} c_i Cov\{x_i u_0\} \\
&+ Cov\{u_0 u_0\}
\end{aligned} \tag{5.4}$$

where $Cov\{u_i u_j\}$ is the auto-covariance between u_i and u_j, $Cov\{v_i v_j\}$ is the auto-covariance between v_i and v_j, $Cov\{x_i x_j\}$ is the auto-covariance between x_i and x_j, $Cov\{u_i v_j\}$ is the cross-covariance between u_i and v_j, $Cov\{u_i x_j\}$ is the cross-covariance between u_i and x_j, and $Cov\{v_i x_j\}$ is the cross-covariance between v_i and x_j.

To derive the cokriging system, the Lagrange multiplier method is used to minimize the error

of variance, and Eq. 5.4 can be rewritten as

$$\mathbf{Var}\{\mathbf{R}\} = \mathbf{w^t C_z w} + \mu(\sum_{i=1}^{n} a_i + \sum_{j=1}^{m} b_j + \sum_{k=1}^{p} c_k - 1) \tag{5.5}$$

where μ is the Lagrange multiplier.

The improved ROCK system can be derived by calculating the partial derivatives of $\mathbf{Var}\{\mathbf{R}\}$ with respect to weights **a**, **b** , **c** and Lagrange multiplier μ , which can be written as

$$\begin{aligned}\frac{\partial Var\{R\}}{\partial a_j} &= 2\sum_{i=1}^{n} a_i Cov\{u_i u_j\} + 2\sum_{i=1}^{m} b_i Cov\{v_i u_j\} \\ &+ 2\sum_{i=1}^{p} c_i Cov\{x_i u_j\} - 2Cov\{u_0 u_j\} + 2\mu_1 \\ &for \quad j = 1,\ldots,n\end{aligned} \tag{5.6}$$

$$\begin{aligned}\frac{\partial Var\{R\}}{\partial b_j} &= 2\sum_{i=1}^{m} b_i Cov\{v_i v_j\} + 2\sum_{i=1}^{n} a_i Cov\{u_i v_j\} \\ &+ 2\sum_{i=1}^{p} c_i Cov\{x_i v_j\} - 2Cov\{u_0 v_j\} + 2\mu_2 \\ &for \quad j = 1,\ldots,m\end{aligned} \tag{5.7}$$

$$\begin{aligned}\frac{\partial Var\{R\}}{\partial c_j} &= 2\sum_{i=1}^{p} b_i Cov\{x_i x_j\} + 2\sum_{i=1}^{n} a_i Cov\{u_i x_j\} \\ &+ 2\sum_{i=1}^{m} b_i Cov\{v_i x_j\} - 2Cov\{u_0 x_j\} + 2\mu_3 \\ &for \quad j = 1,\ldots,p\end{aligned} \tag{5.8}$$

Base on Eq. (5.6) - Eq. (5.8), we get the final cokriging system,

$$\begin{aligned}\sum_{i=1}^{n} a_i Cov\{u_i u_j\} + \sum_{i=1}^{m} b_i Cov\{v_i u_j\} + \sum_{i=1}^{p} c_i Cov\{x_i u_j\} + \mu = Cov\{u_0 u_j\} \\ for \quad j = 1,\ldots,n\end{aligned} \tag{5.9}$$

$$\sum_{i=1}^{n} a_i Cov\{u_i v_j\} + \sum_{i=1}^{m} b_i Cov\{v_i u_j\} + \sum_{i=1}^{p} c_i Cov\{x_i v_j\} + \mu = Cov\{u_0 v_j\} \quad for \quad j = 1, \ldots, m \tag{5.10}$$

$$\sum_{i=1}^{n} a_i Cov\{u_i x_j\} + \sum_{i=1}^{m} b_i Cov\{v_i u_j\} + \sum_{i=1}^{p} c_i Cov\{x_i x_j\} + \mu = Cov\{u_0 x_j\} \quad for \quad j = 1, \ldots, p \tag{5.11}$$

$$\sum_{i=1}^{n} a_i + \sum_{j=1}^{m} b_i + \sum_{k=1}^{p} c_k = 1 \tag{5.12}$$

Note that $Cov\{U_i V_j\} = Cov\{V_i U_j\}$, $Cov\{U_i X_j\} = Cov\{X_i U_j\}$ and $Cov\{V_i X_j\} = Cov\{X_i V_j\}$ We write the matrix form of Eq. (5.9) - Eq. (5.12) as,

$$\begin{pmatrix} C_{uu} & C_{vu} & C_{xu} & \mathbf{1} \\ C_{uv} & C_{vv} & C_{xv} & \mathbf{1} \\ C_{ux} & C_{vx} & C_{xx} & \mathbf{1} \\ \mathbf{1}^T & \mathbf{1}^T & \mathbf{1}^T & \mathbf{0} \end{pmatrix} \begin{pmatrix} \mathbf{a} \\ \mathbf{b} \\ \mathbf{c} \\ \mu \end{pmatrix} = \begin{pmatrix} C_{u_0 u} \\ C_{u_0 v} \\ C_{u_0 x} \\ 1 \end{pmatrix} \tag{5.13}$$

where C_{uu} is the auto-covariance of the primary variable, C_{vv} is the auto-covariance of first secondary variable, and C_{xx} is the auto-covariance of the second secondary variable. C_{uv} is the cross-covariance between primary and first secondary variables, C_{ux} is the cross-covariance between primary and second secondary variables, C_{xv} is the cross-covariance of two secondary variables, μ is the Lagrange multiplier and a, b, and c are weight vectors of primary, first secondary, and second secondary variables to be determined. Note that $C_{uv} = C_{vu}$, $C_{ux} = C_{xu}$, and $C_{xv} = C_{vx}$.

Eq. (5.13) is hereafter referred to as the new cokriging weights function. In next section, the improved cokriging system is applied to a real dataset and evaluated by Leave-one-out cross-validation.

5.3 Case study

The reservoir target is a bitumen-bearing formation which underlies a shale caprock and uncomformably overlies a non-reservoir clastic formation. The objective of this study is shown in Figure 5.1. The interface between the producing reservoir (good sand) and the uneconomic reservoir (bad sand) is difficult to delineate in the stacked seismic data alone, due to the similarity of the rock properties. The study area is located in northern Alberta and includes 11 drilled wells (Figure 5.2). For this investigation, a window from 10 ms above the top reservoir to 10 ms below the base of reservoir was used to produce the averaged seismic attribute slices. To demonstrate the improved ROCK method, the work-flow designed and is displayed in Figure 5.3.

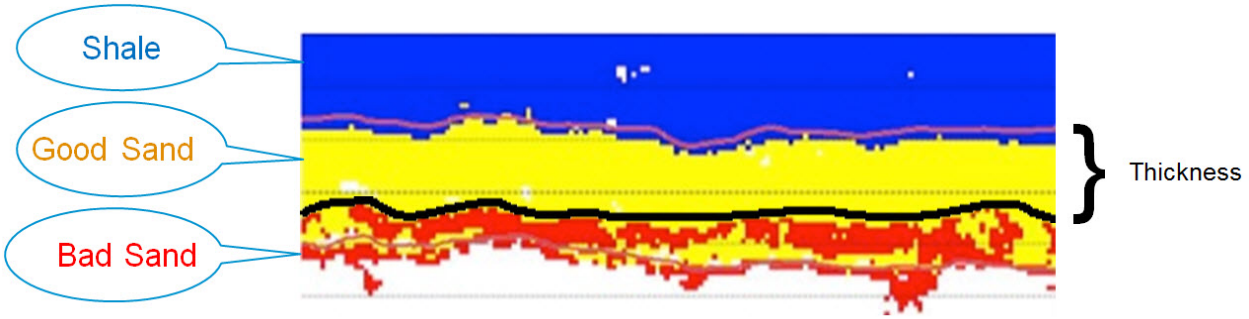

Figure 5.1: The objective of case study

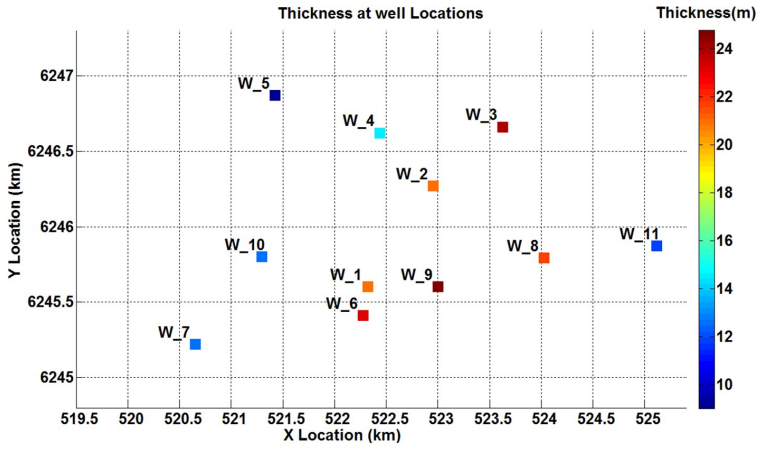

Figure 5.2: Well log distribution and its thickness

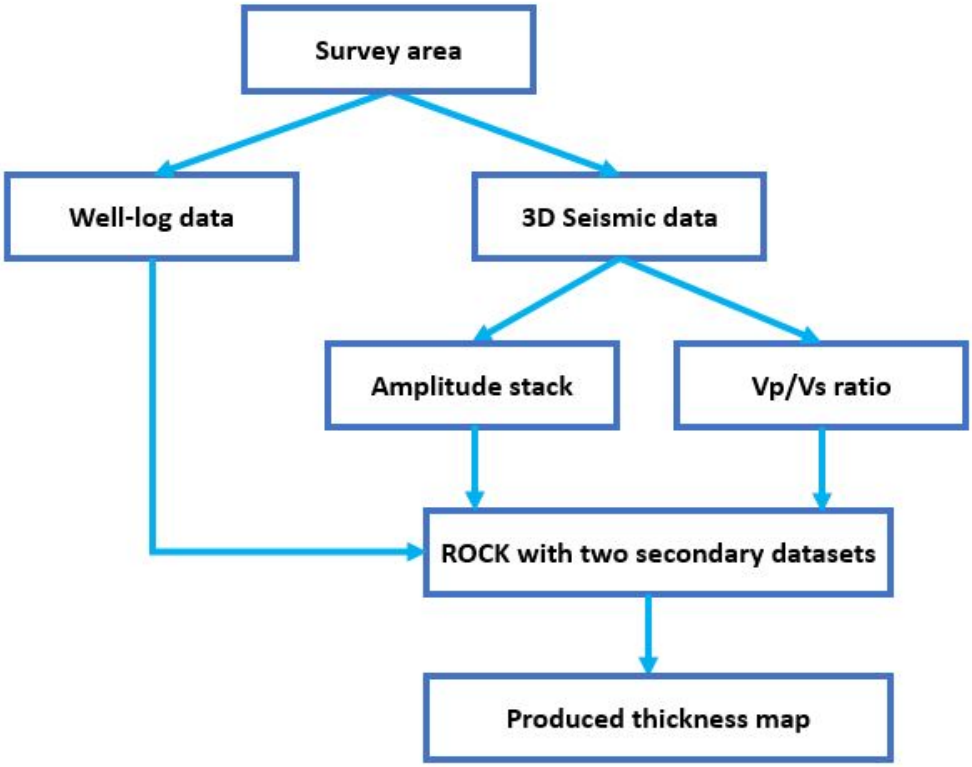

Figure 5.3: Case study work-flow

In this case study, two seismic attributes are utilized as the secondary datasets. One seismic slice was extracted from the raw amplitude of the angle stack in Figure 5.4, and is shown in Figure 5.5. Also the cross-plot between the angle stack amplitude and formation thickness from well logs has a calculated correlation coefficient of 0.49 (Figure 5.8a). Another secondary variable is V_p/V_s ratio, which is shown in Figure 5.7. This attribute was extracted from the joint PP-PS inversion result (Figure 5.6) using the same time window. Its cross-plot against thickness and with a correlation coefficient of 0.58 is shown in Figure 5.8b.

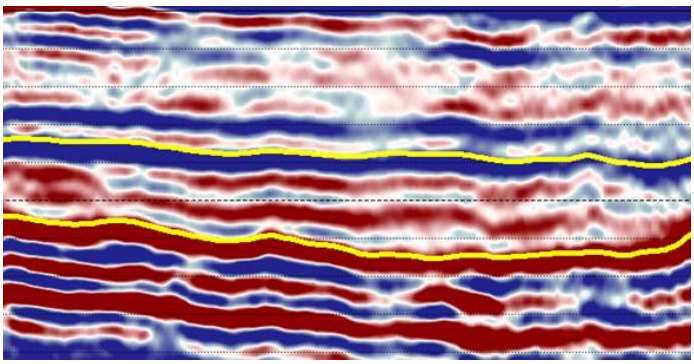

Figure 5.4: Seismic raw amplitude from an angle stack between 8^0 and 29^0

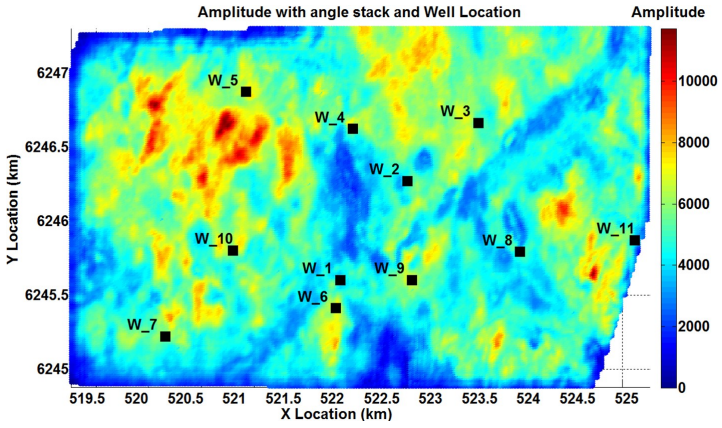

Figure 5.5: Seismic slice of raw amplitude from an angle stack between 8^0 and 29^0, using a window from 10 ms above the reservoir to 10ms below the base clastic formation.

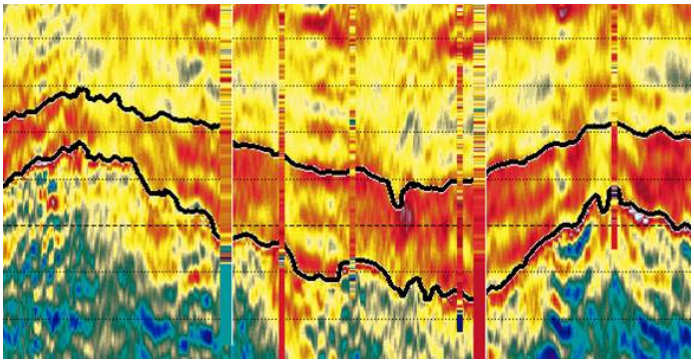

Figure 5.6: Inverted V_p/V_s ratio volume

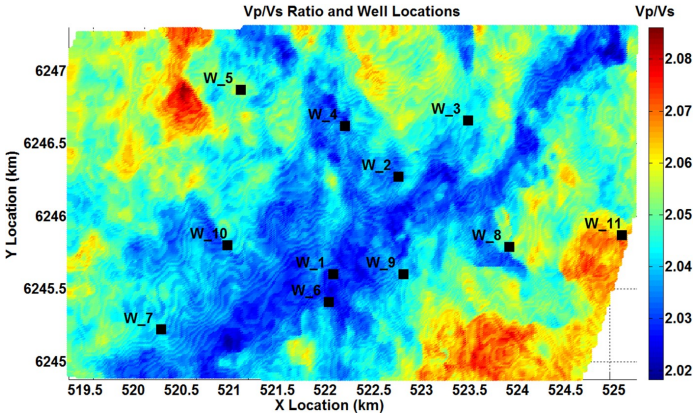

Figure 5.7: Slice of V_p/V_s ratio extracted from an inverted seismic volume using a window from 10ms above the top reservoir to 10ms below the base clastic formation.

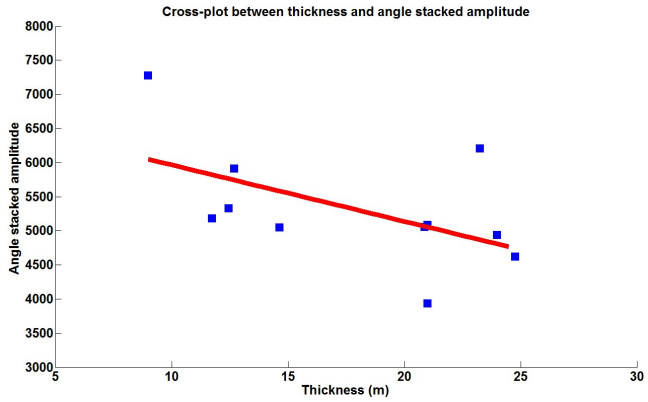

(a) Cross-plot between reservoir depth and angle stack amplitude

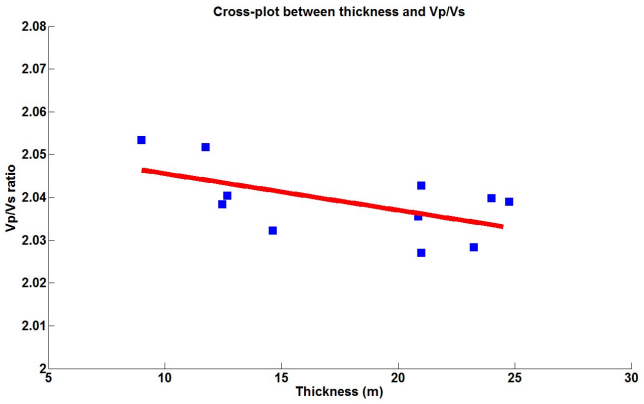

(b) Cross-plot between reservoir depth and V_p/V_S ratio

Figure 5.8: Cross-plots between reservoir thickness derived from well logs and two seismic attributes.

Before applying the improved ROCK algorithm, the variograms of the primary and two secondary variables have been constructed and are shown in Figure 5.9. It shows 6 variograms obtained from the well-log data and two seismic attributes. Figure 5.9a, 5.9e, and 5.9f are auto-variograms of well-log data, inversion, and seismic amplitude, respectively. The cross-variograms are shown in Figure 5.9b, Figure 5.9c, and Figure 5.9d.

After implementing the improved ROCK method, the final predicted thickness and distribution map is displayed in Figure 5.10. To examine the advantages of the predicted thickness map using the improved ROCK method, we also apply the traditional ROCK method with one secondary vari-

able using the angle stack amplitude and V_p/V_s ratio attributes separately, with all other parameters remaining the same. The predicted thickness maps using traditional ROCK are shown in Figure 5.11 and Figure 5.12, as related to the different attributes selected.

Compared to the traditional cokriging results, the final predicted map using the modified cokriging approach does not show the significant differences in the areas where there are more well distributions. However, it shows higher lateral resolution and remarkable differences in those locations where there are less well control points. For a more quantitative analysis, leave-one-out cross-validation was employed to calculate RMS errors, which were calculated from traditional cokriging with inversion, traditional cokriging with seismic amplitude, and the modified cokriging system, are given by the histograms shown in Figure 5.13. Note that this approach shows a lower RMS error than other approaches. This means that the modified cokriging system, involving two well correlated secondary variables, gives a better estimation of the reservoir properties.

A detailed comparison of the improved and traditional ROCK methods shows that improved ROCK with multiple attributes enhances the lateral distribution of the reservoir thickness prediction. The reason is that the two secondary attributes used, data slices of angle stack amplitude and V_p/V_s ratio, are independent of each other and can therefore indicate different reservoir characteristics, which ensures that more geological information is introduced.

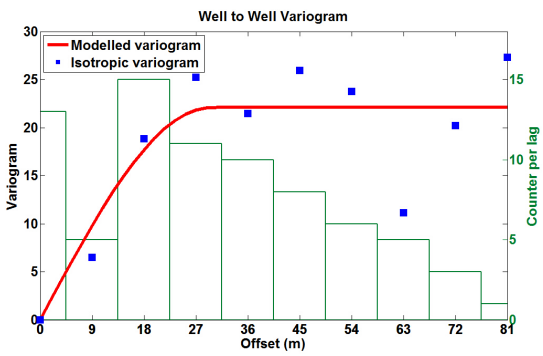

(a) Well to Well Variogram

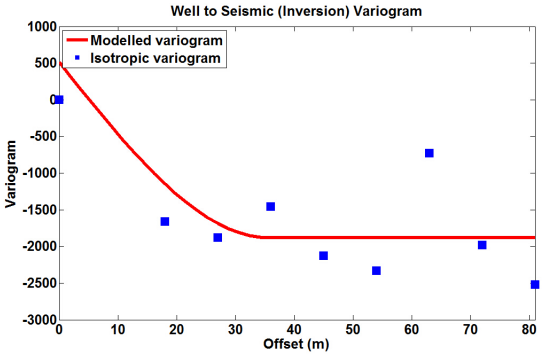

(b) Well to Seismic Inversion Variogram

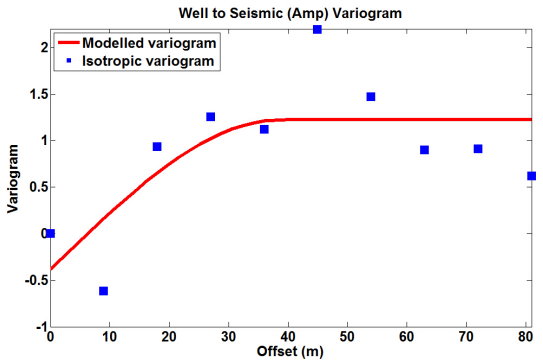

(c) Well to Seismic Amplitude

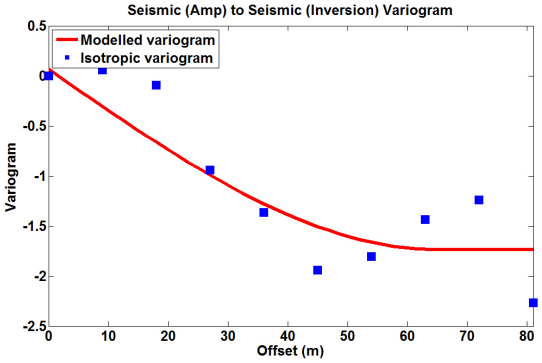

(d) Seismic Amplitude to Inversion Variogram

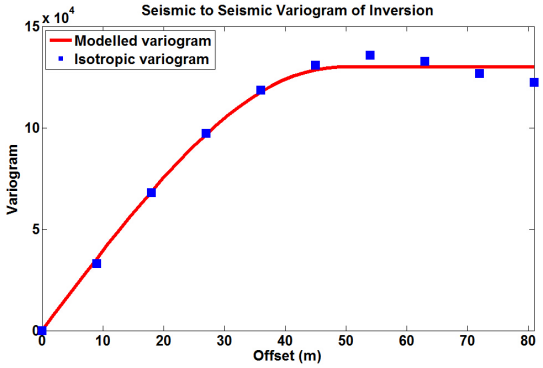

(e) Seismic to Seismic Inversion

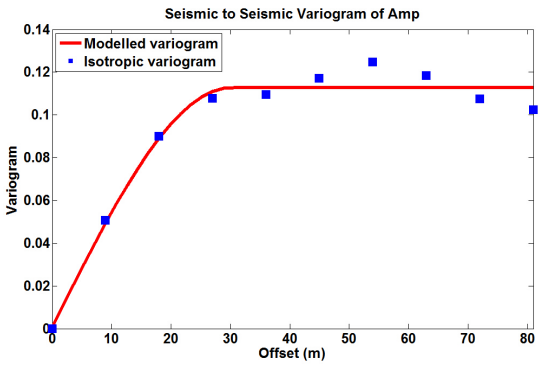

(f) Seismic to Seismic Amplitude

Figure 5.9: Variograms

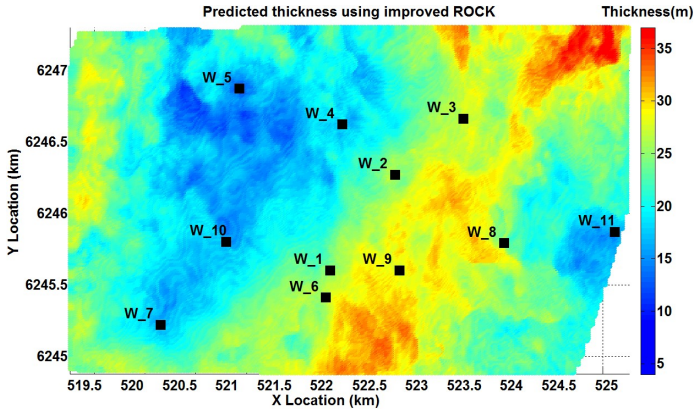

Figure 5.10: Predicted thickness and distribution of the reservoir formation using the improved ROCK method, obtained in considering thickness from the wells as the primary variable, and the angle stack amplitude and V_p/V_S ratio as two secondary variables.

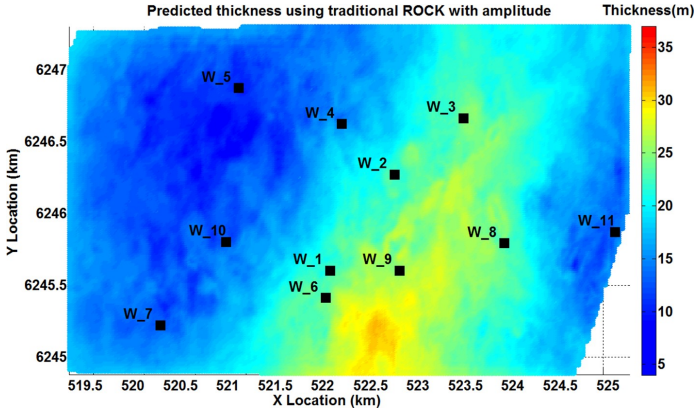

Figure 5.11: Predicted thickness and distribution of the reservoir formation using traditional ROCK with only one secondary variable: angle stack amplitude.

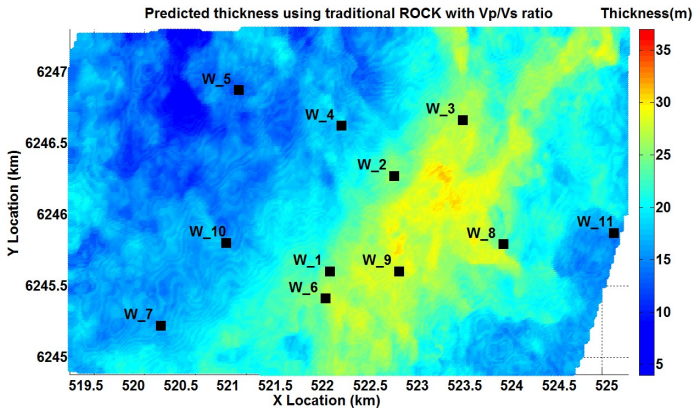

Figure 5.12: Predicted thickness and distribution of the reservoir formation using traditional ROCK with only one secondary variable: V_p/V_S ratio.

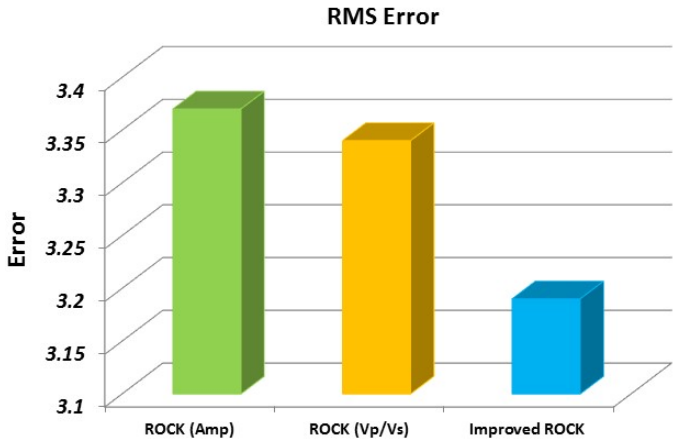

Figure 5.13: Leave-one-out Cross-validation

5.4 Conclusions

Seismic attributes and elastic parameters can be used to delineate different aspects of a reservoir. The inclusion of more independent seismic attributes has the potential to better predict reservoir characteristics. An improved rescaled ordinary cokriging (ROCK) system has been presented to utilize more than one secondary variable. The method could also be extended to other cokriging systems such as simple cokriging (SCK) and ordinary cokriging (OCK).

In this chapter, the improved ROCK method involving two seismic attributes was implemented and used to predict the thickness and distribution of a reservoir in northern Alberta. The estimated thickness map showed that the improved ROCK approach not only increased the accuracy of prediction, but also enhanced the lateral distribution of these parameters. A statistical analysis of this approach let us conclude that the proposed cokriging system has produced an improved lithological prediction of the reservoir.

Chapter 6

Block cokriging with multiple secondary attributes

6.1 Introduction

Block cokriging is employed to estimate an average value over a block area around unsampled points rather than to estimate the value of an unsampled point. It can significantly reduce the computational burden by constructing and solving one cokriging system for each block estimate (Isaaks, E. H. and Srivastava R. M., 1989).

Geostatistical approaches employ spatial correlation to model the lateral variation of the reservoir (Ambrose et al. 2010). For example, the block cokriging method uses a block estimate to provide the average value of a variable within a prescribed local area (Isaaks, E. H. and Srivastava R. M., 1989). There are two reasons to use a block estimate: first, if the study area is large, there exists a significant number of estimated grid points. Second, the zone of interest is dependent on the average of a regionalized variable, such as total organic carbon (TOC).

Block cokriging provides an equivalent predicted value as the estimate value predicted by point cokriging within the block area. For example, the estimate average value of the four points using the point cokriging method in the region (Figure 6.1) yields the same estimate when using the block estimate method.

6.2 Methodology

To take advantage of the inclusion of more seismic attributes, Xu et al. (2016) presented an extended cokriging system for point estimation which can be utilized into any of the forms of cokriging. Suppose $w(x)$ is a point support random function for a whole area, and the true block average

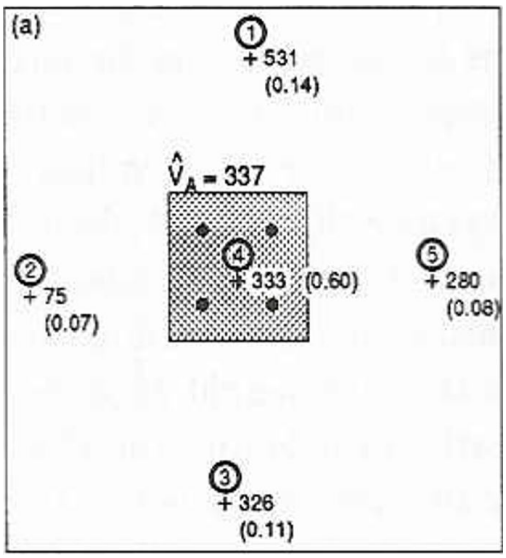

Figure 6.1: Block estimate

in area S at location x is

$$w_S(x_0) = \frac{1}{|S|}\int_S w(x)\,dx \tag{6.1}$$

Similar to the extended cokriging system, the estimator of block cokriging involving two secondary variables at location x_0 in block S can be written as

$$\tilde{w_S}(x_0) = \sum_{i=1}^{n} a_i w_i + \sum_{j=1}^{m} b_j u_j + \sum_{k=1}^{p} c_k v_k \tag{6.2}$$

where a, b, and c are the weight vectors assigned to variables w, u, and v, respectively. Under the unbiasedness condition, the weight vectors are subject to

$$\sum_{i=1}^{n} a_i = 1 \tag{6.3}$$

$$\sum_{j=1}^{m} b_j = 0 \tag{6.4}$$

$$\sum_{k=1}^{p} c_k = 0 \tag{6.5}$$

Therefore, the variance of the estimation error is

$$\begin{aligned}\mathbf{Var}\{\tilde{w_S}(x_0) - w_S(x_0)\} &= \mathbf{w^t C_z w} \\ &= \sum_{i=1}^{n}\sum_{j=1}^{n} a_i a_j C_{w_i w_j} + \sum_{i=1}^{m}\sum_{j=1}^{m} b_i b_j C_{u_i u_j} + \sum_{i=1}^{n}\sum_{j=1}^{n} c_i c_j C_{v_i v_j} \\ &+ 2\sum_{i=1}^{n}\sum_{j=1}^{m} a_i b_j C_{w_i u_j} + 2\sum_{i=1}^{n}\sum_{j=1}^{p} a_i c_j C_{w_i v_j} + 2\sum_{i=1}^{m}\sum_{j=1}^{p} a_i b_j C_{u_i v_j} \\ &- 2\sum_{i=1}^{n} a_i C_{w_i S} - 2\sum_{i=1}^{m} b_i C_{u_i S} - 2\sum_{i=1}^{p} c_i C_{v_i S}\end{aligned} \tag{6.6}$$

with

$$C_{X_i,S} = \frac{1}{|S|}\int_S Cov(X_i, x)dx \tag{6.7}$$

$$C_{S,S} = \frac{1}{|S|^2}\int\int_S Cov(x, y)dxdy \tag{6.8}$$

where $X \in \{w, u, v\}$. Eq. (6.7) and Eq. (6.8) are the point-to-block and block-to-block covariances, respectively, and are calculated by averaging the point-to-point covariances in the area S. In practice, the area is usually discretized into several points to achieve an adequate approximation of the average point-to-block and the block-to-block covariances. Therefore, the number of discretizing points in the area S is the key parameter used to obtain the point-to-block and the block-to-block covariance matrices. It is important to use the same discretization to stabilize the cokriging system in the calculation of the point-to-point and the block-to-block covariances.

Using the Lagrange multiplier approach and minimizing the variance of estimation error by calculating the partial derivatives, the block cokriging weights can be written as

$$\begin{pmatrix} C_{ww} & C_{wu} & C_{wv} & \mathbf{1} & \mathbf{0} & \mathbf{0} \\ C_{uw} & C_{uu} & C_{uv} & \mathbf{0} & \mathbf{1} & \mathbf{0} \\ C_{vw} & C_{vu} & C_{vv} & \mathbf{0} & \mathbf{0} & \mathbf{1} \\ \mathbf{1}^T & \mathbf{0} & \mathbf{0} & \mathbf{0} & \mathbf{0} & \mathbf{0} \\ \mathbf{0} & \mathbf{1}^T & \mathbf{0} & \mathbf{0} & \mathbf{0} & \mathbf{0} \\ \mathbf{0} & \mathbf{0} & \mathbf{1}^T & \mathbf{0} & \mathbf{0} & \mathbf{0} \end{pmatrix} \begin{pmatrix} \mathbf{a} \\ \mathbf{b} \\ \mathbf{c} \\ -\mu_\mathbf{1} \\ -\mu_\mathbf{2} \\ -\mu_\mathbf{3} \end{pmatrix} = \begin{pmatrix} C_{wS} \\ C_{uS} \\ C_{vS} \\ 1 \\ 0 \\ 0 \end{pmatrix} \tag{6.9}$$

where C_{XY} are the point-to-point covariance matrices, which contains the spatial relationships between primary and two secondary variables related to its subscripts, $X, Y \in \{w,u,v\}$. w is the primary data, u and v are two different secondary variables. C_{XS} are the point-to-block covariance matrices between all given data and the estimated block, which can be calculated by Eq. (6.7).

To compute the block cokriging weights, Eq. (6.9) can be rewritten as

$$\begin{pmatrix} \mathbf{a} \\ \mathbf{b} \\ \mathbf{c} \\ -\mu_1 \\ -\mu_2 \\ -\mu_3 \end{pmatrix} = \begin{pmatrix} C_{ww} & C_{wu} & C_{wv} & \mathbf{1} & \mathbf{0} & \mathbf{0} \\ C_{uw} & C_{uu} & C_{uv} & \mathbf{0} & \mathbf{1} & \mathbf{0} \\ C_{vw} & C_{vu} & C_{vv} & \mathbf{0} & \mathbf{0} & \mathbf{1} \\ \mathbf{1}^T & \mathbf{0} & \mathbf{0} & \mathbf{0} & \mathbf{0} & \mathbf{0} \\ \mathbf{0} & \mathbf{1}^T & \mathbf{0} & \mathbf{0} & \mathbf{0} & \mathbf{0} \\ \mathbf{0} & \mathbf{0} & \mathbf{1}^T & \mathbf{0} & \mathbf{0} & \mathbf{0} \end{pmatrix}^{-1} \begin{pmatrix} C_{wS} \\ C_{uS} \\ C_{vS} \\ 1 \\ 0 \\ 0 \end{pmatrix} \tag{6.10}$$

The block cokriging variance can be simplified in terms of weights and is given by

$$\mathbf{Var} = C_{SS} - (a^T C_w S + b^T C_u S + c^T C_v S) \tag{6.11}$$

In the implementation of block cokriging, lookup covariance tables are created to contain all the previously calculated covariance values which will be reused in calculation. The computational burden is significantly reduced when the pre-calculated covariance tables are utilized. However, the matrix on the left side of Eq. (6.9) can still be too large to be convenient to use in computations. To solve that, a neighbourhood search strategy is applied in the block cokriging procedure, which is shown in Figure 6.2.

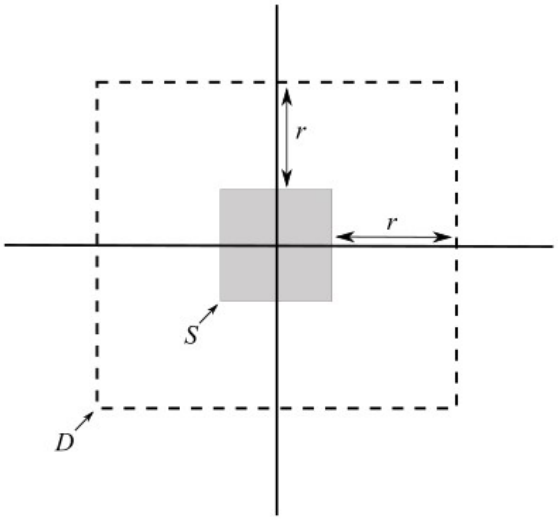

Figure 6.2: The neighborhood strategy for block cokriging system. S is the estimated block. D is the search area for block S, $\{w,u,v\} \in D$. r is the range of semi-variogram.

6.3 Case study

In this case study, the modified block cokriging method is applied to a producing shale gas reservoir in British Columbia, Canada for predicting total organic carbon (TOC). TOC is the weight percentage of carbon in the source rock. Quantification of TOC plays a significant role for identifying potential organic shale reservoirs (Memarsadeghi, N. and Mount, D.M., 2007). Ambrose et al. (2010) demonstrated that the quantity of TOC is related to the quantity of gas shales, as the producible pore fluids are in the organic matter. Estimating TOC is difficult in a lateral sense away from the borehole. This is because although TOC can be measured from core data by geochemical analysis in the laboratory or calculated empirically using well-log data, it cannot be obtained directly in the area between boreholes. Improved seismic acquisition and quantitative seismic processing techniques, which include the amplitude with offset Amplitude Versus Offset (AVO) technique, now offer us an opportunity to estimate TOC laterally away from the wells using seismic data.

In order to predict TOC in a shale gas play using the improved block cokriging method, we first need to determine which elastic parameters and seismic attributes are the best indicators of TOC. Inverted elastic parameters, such as V_p/V_s ratio extracted from prestack inversion, have been

shown to be associated with TOC in rock physics modelling (Qin et al., 2014). Zhu et al.,(2012) described that an increase in the TOC generally results in a lower V_p/V_s ratio. Additionally, Neto et al., (2016) showed that seismic amplitude can be a predictor of TOC. Loseth et al. (2011) also discussed the relationship between the TOC profile and the seismic amplitude response. Next, we need to consider the size of the survey. The number of estimated grid points in the survey area of 90,000 m^2 is over 52,000, which could cause the prediction to become computationally expensive if done with the traditional geostatistical approach in a point estimate manner. Therefore, the block estimate is more suitable for this objective, as the spatial area of interest to predict TOC is the average in a region rather than at one single point.

The study area is located in British Columbia, Canada and includes eight producing wells. Based on previous research, we are focusing on a formation that is a shale play targeting dry gas. TOC is considered as the primary variable, and is computed as the average value between the two picked zones of interest extracted from each well.

Figure 6.3 shows the distribution of the wells in the survey area and the value of TOC at each well location is indicated by the color bar. To evaluate the improved block cokriging system, two secondary variables are required. Prestack inversion was applied to generate a number of seismic attribute volumes for the selection of secondary variables. Then, a 13 ms window above the base of target zone of interest was used to create the relevant data slices.

The average V_p/V_S ratio over the time window shown in Figure 6.4 was selected as the first secondary variable for the cokriging system due to its high correlation with TOC (equal to -0.69). The second secondary variable was the amplitude of an angle stack displayed in Figure 6.5, which has a correlation coefficient of -0.70. The relationships between TOC and two secondary variables are analyzed by cross-plots shown on the left of Figure 6.6 and right of 6.6, respectively. Figure 6.6 shows negative relationships between both V_p/V_S ratio and angle-stacked raw amplitude and TOC.

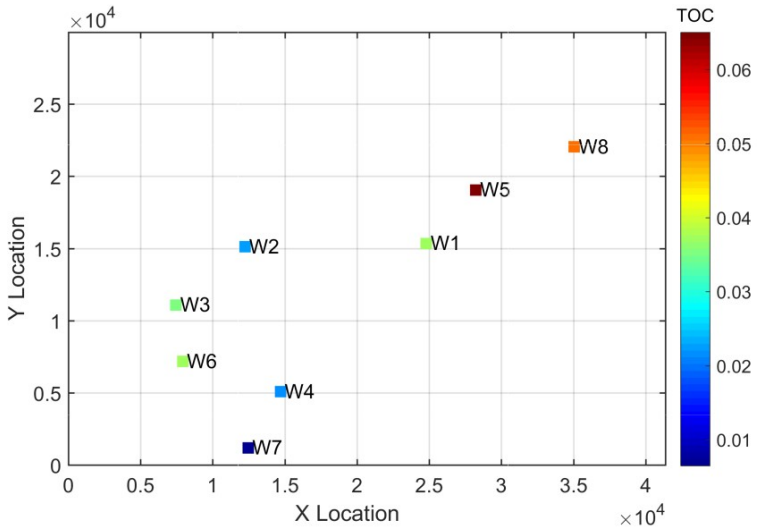

Figure 6.3: TOC distribution at all well locations.

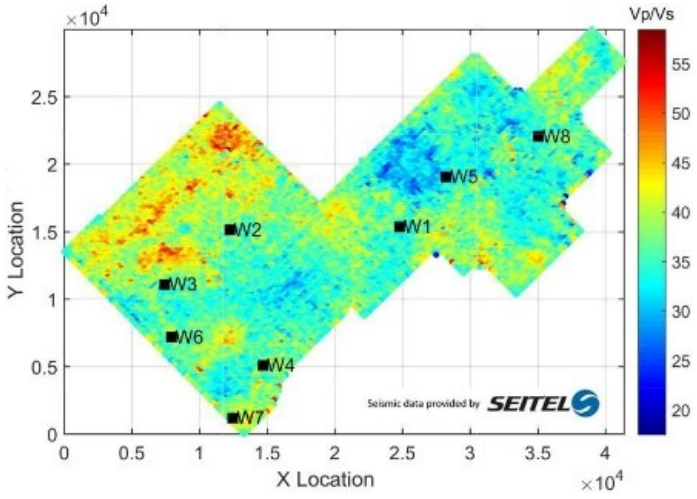

Figure 6.4: The average V_p/V_S ratio distribution and well locations.

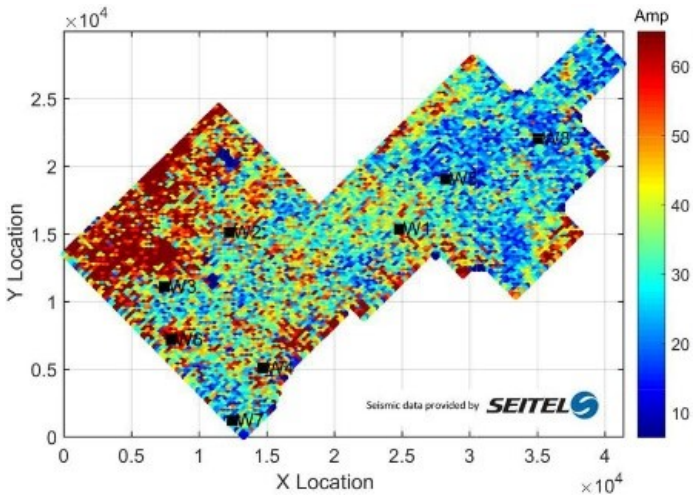

Figure 6.5: The raw amplitude of an angle stack and well locations.

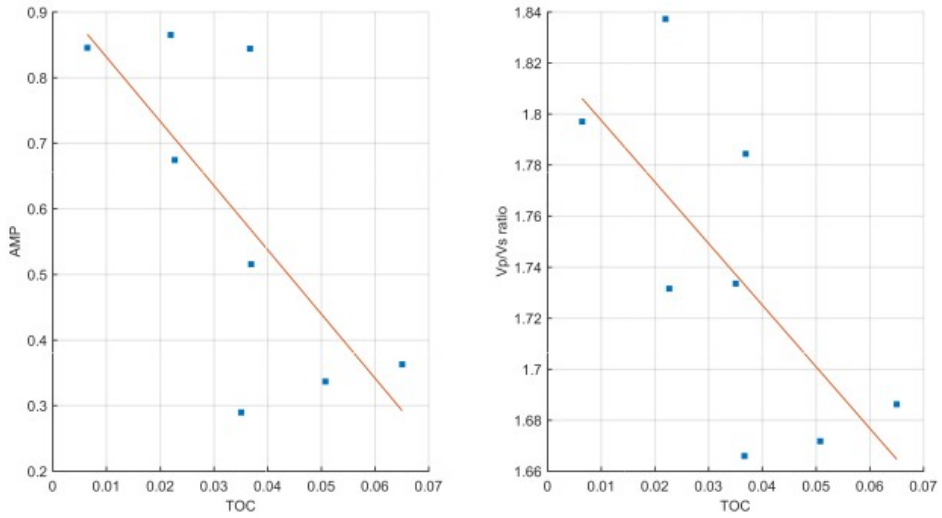

Figure 6.6: Cross-plots between two secondary variables and TOC at well locations. Left: cross–plot of angle-stacked raw amplitude and TOC; Right: cross-plot of V_p/V_S ratio and TOC.

The block cokriging method is based on the spatial variation which is quantified by the semi-variogram. The auto semi-variograms and cross semi-variograms of the primary and two secondary variables have been computed and displayed in Figure 6.7. To best utilize the calculated covariance from previous calculations, and to avoid the repetitive computation of covariance at the same location, pre-calculated covariance lookup tables were employed.

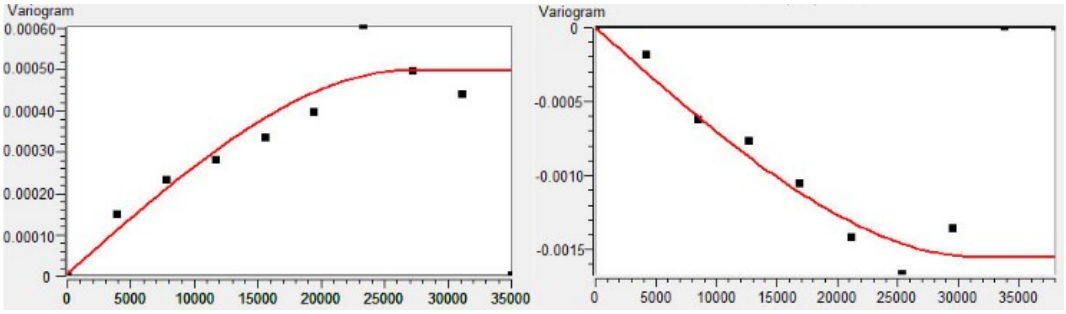

(a) and (d)

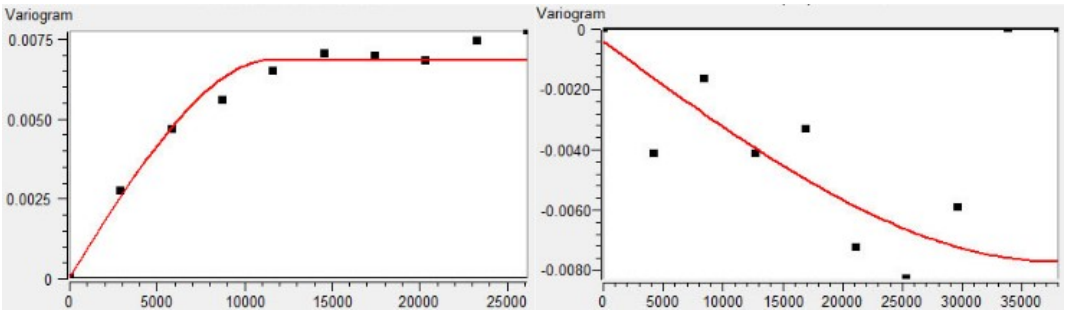

(b) and (e)

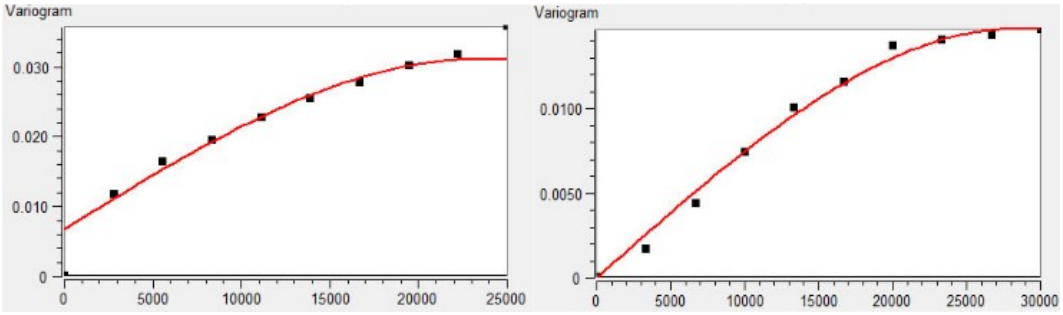

(c) and (f)

Figure 6.7: Semi-variograms of two secondary variables: V_p/V_S ratio and angle-stacked amplitude, and primary varaible: TOC from well-log data, where (a) is TOC to TOC, (b) is V_p/V_S to V_p/V_S , (c) is amplitude to amplitude, (d) is TOC to V_p/V_S , (e) is TOC to amplitude, and (f) is V_p/V_S to amplitude.

Each $16 \times 24m^2$ block has been discretized by 384 points to obtain an adequate and stabilized the average point-to-block and block-to-block covariances by Eq. (6.7) and Eq. (6.8). Then, the TOC estimation in the zone of interest in the formation is found by computing the improved block

cokriging weights using Eq. (6.10). Figure 6.8 shows the final predicted result, the estimated average TOC values in the zone of interest using improved block cokriging. Compared to the distribution of V_p/V_S ratio and angle-stacked raw amplitude displayed in Figure 6.4 and Figure 6.5, the lateral variation of the TOC estimate in Figure 6.8 demonstrates an approximate negative linear characteristic, which is also implied by the cross-plots shown in Figure 6.6.

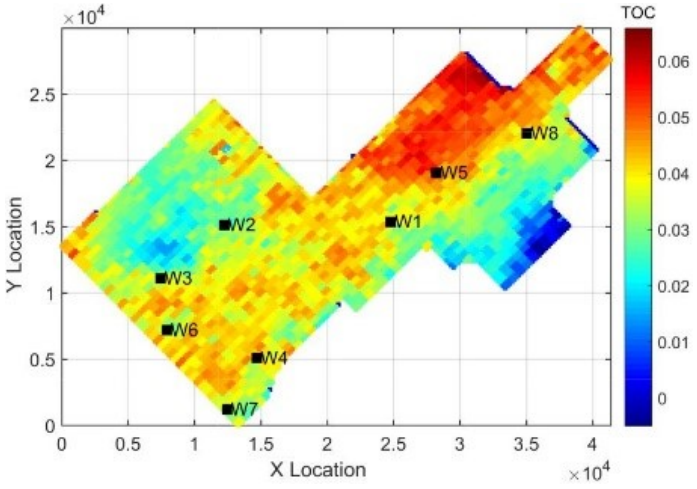

Figure 6.8: The TOC estimation generated by the improved block cokriging system within $16x24m^2$ blocks.

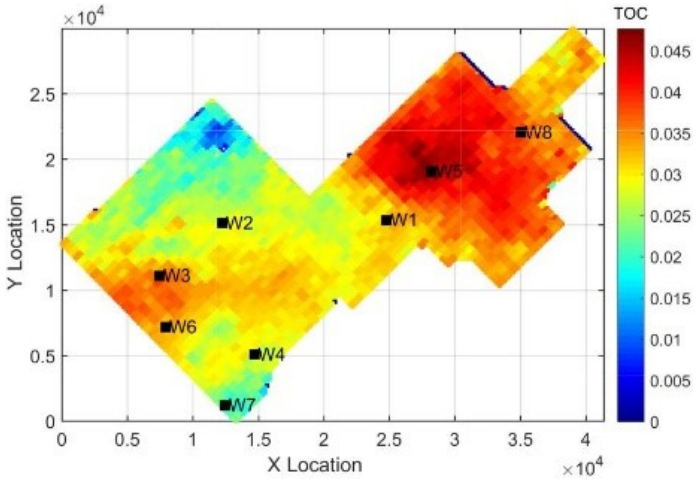

Figure 6.9: The TOC estimation using the traditional block cokriging with average V_p/V_S ratio.

To examine what benefits the second secondary variable brings to the improved block cokriging system, the traditional block cokriging has been performed, which allows for only one secondary

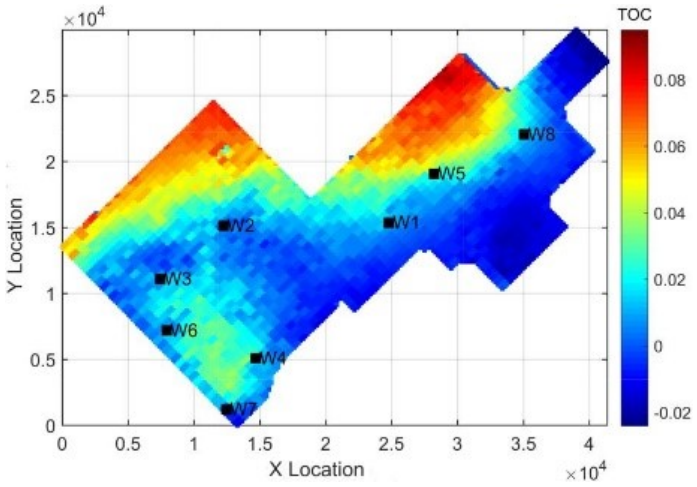

Figure 6.10: The TOC estimation using the traditional block cokriging with angle stacked raw amplitude.

data within the same block size. Figure 6.9 illustrates the TOC estimation using traditional block cokriging with the V_p/V_S ratio. The left side of Figure 6.9 shows a similar distribution of TOC as the estimation by improved block cokriging shown in Figure 6.8. However, the variation in top right of Figure 6.9 is not consistent with the variation of V_p/V_S ratio shown in Figure 6.4, which is likely due to the size of the block used. Beyond that, compared to the TOC distribution at the well locations (Figure 6.3), the TOC values using traditional cokriging with only V_p/V_S ratio is underestimated.

The TOC estimation using the traditional block cokriging with only the angle-stacked amplitude is shown in Figure 6.10. The left side of Figure 6.10 shows a decreasing trend in TOC from top to bottom which is not consistent with the negative linear relationship described in the cross-plot of angle-stacked amplitude and TOC shown on the left of Figure 6.6. This possibly arises from the instability of the point-to-block and block-to-block covariance calculations in the block size. In addition, the instability also increases the risk of generating negative values.

Quantitative analysis of the estimated results between the traditional method with only one secondary variable and improved block cokriging involving two secondary variables is evaluated by calculating the mean-square-error (MSE) at all well locations. The comparison of errors illustrated in Figure 6.11 is in conformity with the qualitative analysis described previously, and demonstrates

that the improved method has the lowest error.

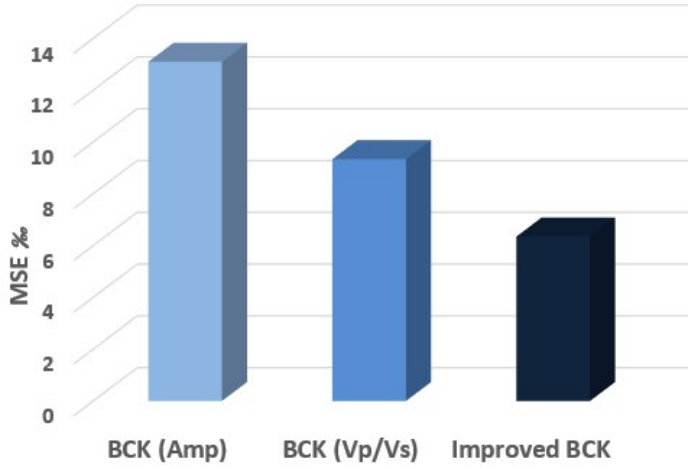

Figure 6.11: Mean-square-error analysis of estimated results using traditional and improved block cokriging at all well locations.

6.4 Conclusions

Understanding the spatial continuity of TOC provides information about the hydrocarbon storage capability of shale gas plays. In this study, an improved block cokriging system with two secondary variables has been presented and applied to an unconventional reservoir to predict TOC. By analyzing the estimate created by traditional and improved block cokriging, the modified approach improves the accuracy of the estimate, reduces the risk of generating negative values, and stabilizes the block cokriging system. The use of both seismic attributes and elastic parameters can provide more geological information about reservoir properties. We concluded that there is the potential of superior reservoir characterization by introducing more independent seismic attributes, especially ones which are highly correlated with the primary variable. Additionally, by pre-calculating the covariance lookup tables for the primary and secondary variables, and by applying the neighbourhood search strategy, this method was able to be used in computations, especially on large datasets.

Chapter 7

Sequential Gaussian simulation using multi-variable cokriging

7.1 Introduction

Uncertainty analysis is a key element in reservoir property prediction, and many techniques have been developed to perform this analysis, such as geostatistical inversion and simulation. In the stochastic approach, sequential simulation is used to generate a series of equivalent and possible realizations which reflect the natural variability and heterogeneity of reservoir properties. The conditional mean and covariance are the key parameters in sequential simulation, and are usually obtained by the least-squares method. As Dermanis (1984) and Ligas and Kulczycki (2010) illustrated, the least-squares method is equivalent to the simple geostatistical methods (simple (co)kriging). Ordinary (co)kriging, an alternate solution to the geostatistical problem, provides a superior approach by utilizing the local mean instead of the global mean used by least-squares or simple (co)kriging.

Previous research work has shown that the least-squares method and simple (co)kriging method are equivalent to conditional expectation in the posterior distribution. This indicates that the advantage of ordinary approach, compared to the simple system, may also be superior to a least-squares approach. Therefore, the extended rescaled ordinary cokriging (ROCK) method is used to implement sequential simulation instead of the least-squares method, which means that the posterior mean and variance of sequential simulation are computed by ROCK. Finally, this approach is applied to Black-foot 3C-3D dataset for porosity simulation.

7.2 Methodology

Any estimation, interpolation, projection or transformation problem, based on a given data **d**, can be treated as the inversion problem in which we solve for the model parameters that generates the data using the equation (Claerbout,1992):

$$\mathbf{d} = \mathbf{G}\mathbf{m} \tag{7.1}$$

where **d** is the observed data, **m** represents the model parameters, and **G** is a projection operator. Therefore, the key is to find the best-fit model **m** for the operator **G** using the observed data **d**. The classical approach to solve Eq. (7.1) is to use the unbiased minimum error variance criteria between the data and model, which turns the above problem into least-squares prediction. A unique, best-fit estimate by the least-squares method can be described as the weighted combination of the prior information where three criteria are met: *linearity*, *unbiasedness*, and *minimum error variance*. The aim is to compute a set of weights satisfying these three criteria, which turns the estimation into the simple geostatistical problem. In fact, least-squares prediction is equivalent to the interpolated result using a simple geostatistical system, such as a simple kriging or simple cokriging (Dermanis, 1984; Ligas and Kulczycki, 2010). Tarantola (2005) demonstrated that the least-squares method (Eq. 7.1) can also be described using the posterior Gaussian probability density given by:

$$P(\mathbf{m}|\mathbf{d}) = kexp\left[-\frac{1}{2}(\mathbf{m}-\boldsymbol{\mu}_{m|d})^T\boldsymbol{\Sigma}_{m|d}^{-1}(\mathbf{m}-\boldsymbol{\mu}_{m|d})\right] \tag{7.2}$$

Where k is a scale factor and the conditional mean is

$$\boldsymbol{\mu}_{m|d} = \boldsymbol{\mu}_m + (\mathbf{G}\mathbf{C}_m)^T(\mathbf{G}\mathbf{C}_m\mathbf{G}^T + \mathbf{C}_d)^{-1}(\mathbf{d}-\boldsymbol{\mu}_d) \tag{7.3}$$

the conditional covariance is

$$\boldsymbol{\Sigma}_{m|d} = \mathbf{C}_m - \mathbf{C}_m\mathbf{G}^T(\mathbf{G}\mathbf{C}_m\mathbf{G}^T + \mathbf{C}_d)^{-1}(\mathbf{d}-\boldsymbol{\mu}_d) \tag{7.4}$$

where, $\boldsymbol{\mu}_m$ and $\boldsymbol{\mu}_d$ are the mean vectors for model and given data respectively, $\mathbf{C}_m$ and $\mathbf{C}_d$ are the model and data covariance matrices. Here, the conditional mean $\boldsymbol{\mu}_{m|d}$ and covariance $\boldsymbol{\Sigma}_{m|d}$ are identical to the simple kriging or simple cokriging mean and covariance.

Tarantola (2005) and Hansen et al. (2006) also showed that posterior Gaussian probability density distribution can be adopted for **N** given datasets. Assume there are known model parameters $\mathbf{\Phi}_0(\mathbf{x}_i)$ at m locations ($\mathbf{x}_i \in \{\mathbf{x}_1, \mathbf{x}_2, \ldots, \mathbf{x}_m\}$) and two given datasets **A** and **I**. Based on Eq. (7.1), the projection between model parameters ($m = \mathbf{\Phi}$) and two given datasets can be written as

$$\mathbf{d} = \begin{bmatrix} \mathbf{\Phi}_0 \\ \boldsymbol{A} \\ \boldsymbol{I} \end{bmatrix}, \mathbf{C}_d = \begin{bmatrix} \mathbf{C}_{\mathbf{\Phi}\mathbf{\Phi}} & \mathbf{C}_{\mathbf{\Phi}\boldsymbol{A}} & \mathbf{C}_{\mathbf{\Phi}\boldsymbol{I}} \\ \mathbf{C}_{A\mathbf{\Phi}} & \mathbf{C}_{\boldsymbol{A}\boldsymbol{A}} & \mathbf{C}_{\boldsymbol{A}\boldsymbol{I}} \\ \mathbf{C}_{\boldsymbol{I}\mathbf{\Phi}} & \mathbf{C}_{\boldsymbol{I}\boldsymbol{A}} & \mathbf{C}_{\boldsymbol{I}\boldsymbol{I}} \end{bmatrix}, \boldsymbol{\mu}_0 = \begin{bmatrix} \boldsymbol{\mu}_{\mathbf{\Phi}} \\ \boldsymbol{\mu}_{\boldsymbol{A}} \\ \boldsymbol{\mu}_{\boldsymbol{I}} \end{bmatrix} \tag{7.5}$$

The equivalent extended simple cokriging system (Xu et al., 2015) can be written as

$$\begin{bmatrix} \mathbf{C}_{\mathbf{\Phi}\mathbf{\Phi}} & \mathbf{C}_{\mathbf{\Phi}\boldsymbol{A}} & \mathbf{C}_{\mathbf{\Phi}\boldsymbol{I}} \\ \mathbf{C}_{\boldsymbol{A}\mathbf{\Phi}} & \mathbf{C}_{\boldsymbol{A}\boldsymbol{A}} & \mathbf{C}_{\boldsymbol{A}\boldsymbol{I}} \\ \mathbf{C}_{\boldsymbol{I}\mathbf{\Phi}} & \mathbf{C}_{\boldsymbol{I}\boldsymbol{A}} & \mathbf{C}_{\boldsymbol{I}\boldsymbol{I}} \end{bmatrix} \begin{bmatrix} \boldsymbol{\lambda}_1 \\ \boldsymbol{\lambda}_2 \\ \boldsymbol{\lambda}_3 \end{bmatrix} = \begin{bmatrix} \mathbf{C}_{\mathbf{\Phi}_0\mathbf{\Phi}} \\ \mathbf{C}_{\mathbf{\Phi}_0\boldsymbol{A}} \\ \mathbf{C}_{\mathbf{\Phi}_0\boldsymbol{I}} \end{bmatrix} \tag{7.6}$$

Solving the problem involves the following steps:

1. Sort the estimated locations into a random sequence $\{\mathbf{x}_1, \mathbf{x}_2, \ldots, \mathbf{x}_n\}$.

2. Visit the grid point $\mathbf{x}_j$ according to the path generated in step 1.

3. Calculate the conditional mean and covariance at visited location $\mathbf{x}_j$ based on known $\mathbf{\Phi}_0$ and pre-simulated model parameters $\mathbf{\Phi}(\mathbf{x}_1, ..., \mathbf{x}_{j-1})$ and two given datasets (**A** and **I**), by performing least-squares or simple geostatistical methods.

4. Build the posterior probability distribution $P\left\{\mathbf{\Phi}(\mathbf{x}_j)|\mathbf{\Phi}_0, \mathbf{A}, \mathbf{I}, \mathbf{\Phi}(\mathbf{x}_1, ..., \mathbf{x}_{j-1})\right\}$, and draw a random value. Then, put this simulated value at location $\mathbf{x}_j$ into the known dataset.

5. Move to the next location $\mathbf{x}_{j+1}$ in the sequence, and repeat step 2-4 until the last grid point in the sequence is encountered.

The procedure proposed to implement sequential Gaussian simulation (SGS) is inspired by the extended rescaled ordinary cokriging system as described by Xu et al. (2016).

$$\begin{bmatrix} \mathbf{C}_{\boldsymbol{\Phi}\boldsymbol{\Phi}} & \mathbf{C}_{\boldsymbol{\Phi A}} & \mathbf{C}_{\boldsymbol{\Phi I}} & \mathbf{1} \\ \mathbf{C}_{\boldsymbol{A\Phi}} & \mathbf{C}_{\boldsymbol{AA}} & \mathbf{C}_{\boldsymbol{AI}} & \mathbf{1} \\ \mathbf{C}_{\boldsymbol{I\Phi}} & \mathbf{C}_{\boldsymbol{IA}} & \mathbf{C}_{\boldsymbol{II}} & \mathbf{1} \\ \mathbf{1}^T & \mathbf{1}^T & \mathbf{1}^T & \mathbf{0} \end{bmatrix} \begin{bmatrix} \boldsymbol{\lambda}_1 \\ \boldsymbol{\lambda}_2 \\ \boldsymbol{\lambda}_3 \\ \mu \end{bmatrix} = \begin{bmatrix} \mathbf{C}_{\boldsymbol{\Phi}_0\boldsymbol{\Phi}} \\ \mathbf{C}_{\boldsymbol{\Phi}_0\boldsymbol{A}} \\ \mathbf{C}_{\boldsymbol{\Phi}_0\boldsymbol{I}} \\ \mathbf{1} \end{bmatrix} \tag{7.7}$$

Detailed comparisons between simple, ordinary, and rescaled ordinary methods for kriging and cokriging were discussed by Goovaerts (1998). He concluded that, instead of a stationary mean in a simple cokriging system, the rescaled ordinary cokriging (ROCK) method utilizes the estimated local mean. Furthermore, the unbiasedness constraint applied to the weight vector reduces the risk of producing unacceptable estimates, such as singular or negative values (Goovaerts, 1998; Xu et al., 2016). In this chapter, rather than using a least-squares or simple (co)kriging system, performing SGS with the extended ROCK system (SGS-extended ROCK) to obtain the conditional mean and covariance brought practical benefits.

In the implementation of SGS, the covariance matrix becomes larger and larger as the number of iterations increases, which makes the approach time consuming and potentially incalculable. However, as shown by Deutsch et al. (1998), data far beyond the range of the semi-variogram has little contribution to the mean and covariance of the posterior probability distribution. Therefore, by omitting data beyond the range of the semi-variogram, the covariance matrix of the extended ROCK method can be made computationally manageable. To best utilize the calculated covariance from previous iterations, and to avoid the repetitive computation of covariance at the same location, pre-calculated covariance lookup tables are employed.

7.3 Case study

In this study, SGS-extended ROCK will be applied to the Black-foot 3C-3D dataset to simulate porosity. The well distribution with porosity values is displayed in Figure 7.1. Two data slices, the data slice of RMS amplitude (Figure 7.2) and the data slice of acoustic impedance inversion of the seismic data (Figure 7.3), were selected as the two secondary datasets for this improved method. This was due to the high correlation between porosity and these two seismic attributes.

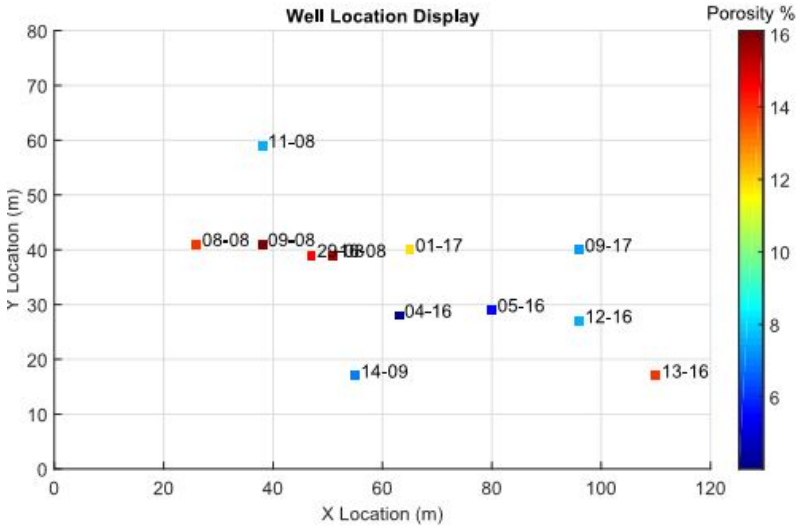

Figure 7.1: Well distribution with porosity values

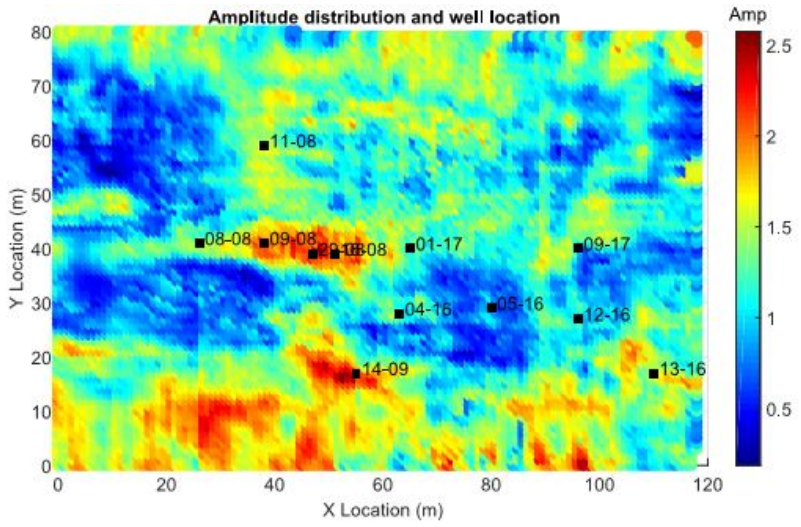

Figure 7.2: Data slice of RMS amplitude

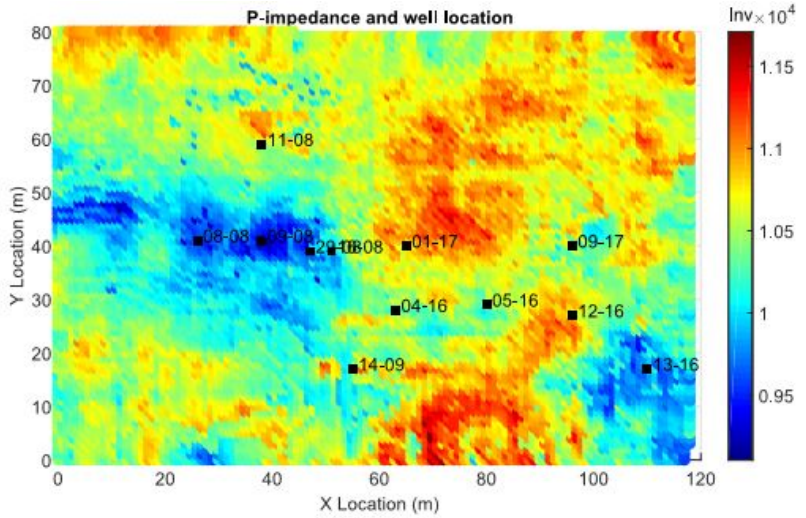

Figure 7.3: Data slice of acoustic impedance inversion

SGS used the procedures illustrated previously, except that conditional mean and variance calculations were done using an extended ROCK system. One hundred realizations were generated, six of which are shown in Figure 7.4.

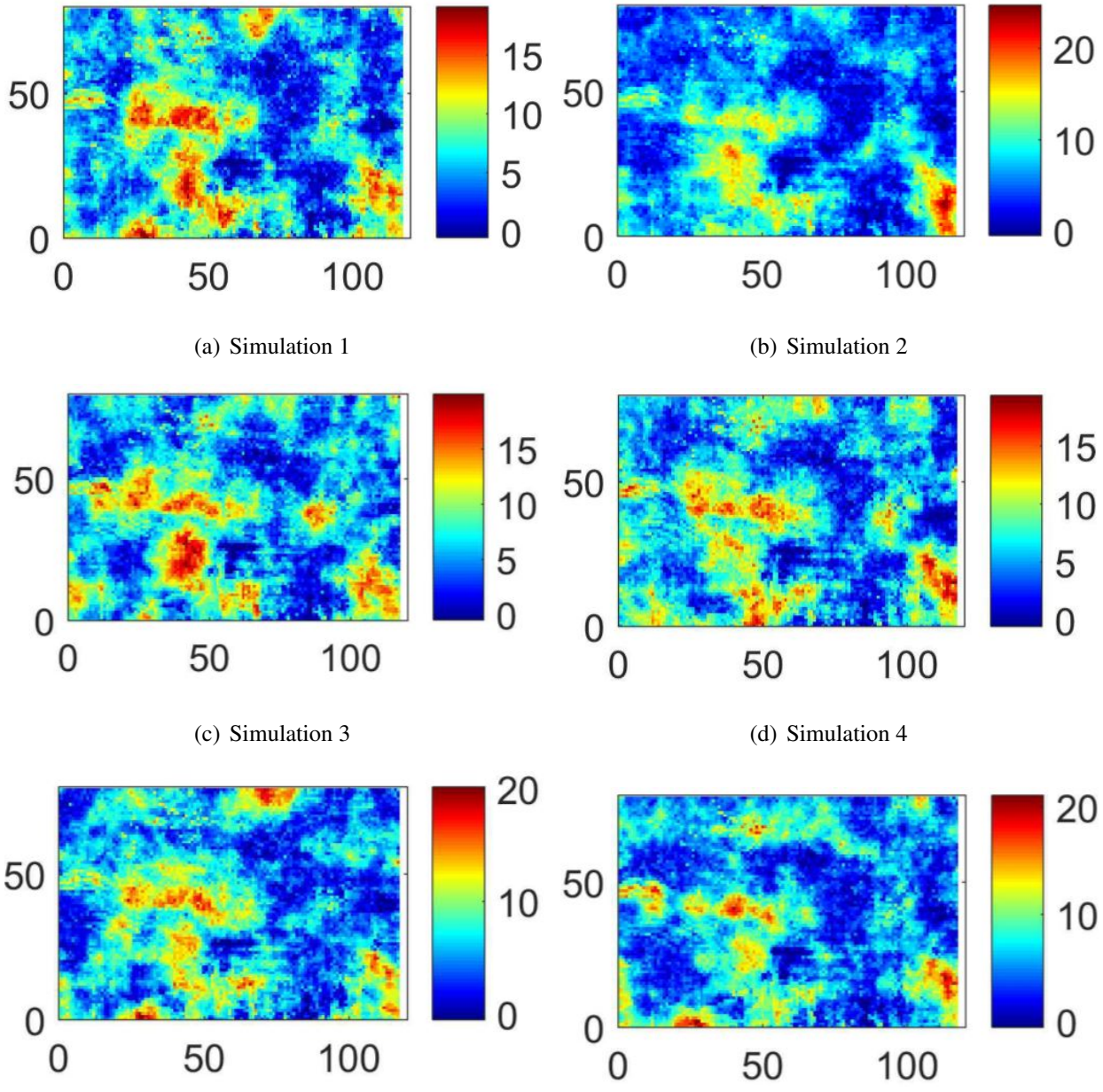

(a) Simulation 1

(b) Simulation 2

(c) Simulation 3

(d) Simulation 4

(e) Simulation 5

(f) Simulation 6

Figure 7.4: Simulations

All the realizations shown in Figure 7.4 correctly delineate the major porosity trends compared

to the "model parameters" (Figure 7.1). This reinforces the validity of the sequential Gaussian simulation with the extended rescaled cokriging system (SGS-extended ROCK). The mean map of all realizations is shown in Figure 7.5. An additional benefit of the SGS method is the generation of probability map. For instance, Figure 7.6 shows the probability of porosity greater than 10%. To analyze the influence of extended ROCK system, the SGS with least-squares method(SGS-LS) was also implemented. The difference between SGS-extended ROCK and SGS-LS is shown in Figure 7.7. The error map verifies the observation made by Goovaerts(1998) that the departures of the estimated primary and all secondary local means from stationary means result in the differences between simple cokriging and rescaled ordinary cokriging. The related error difference between extended simple cokriging(SCK) and extended rescaled ordinary cokriging (ROCK) at a particular location $\mathbf{x}$, can be written as

$$Z_{ROCK}(\mathbf{x}) - Z_{SCK}(\mathbf{x}) = \left[\lambda_1^{SCK} + \lambda_2^{SCK} + \lambda_3^{SCK}\right] [m_{ROCK}(\mathbf{x}) - m_1] \tag{7.8}$$

where $Z_{ROCK}(\mathbf{x})$ and $Z_{SCK}(\mathbf{x})$ denote estimations calculated from extended ROCK and SCK systems. m_1 and $m_{ROCK}(\mathbf{x})$ represent the stationary mean and local mean, respectively. Eq. (7.8) indicates that the extended ROCK estimates are higher than extended SCK (or LS) estimates where the local mean is higher than the global mean, and vice versa.

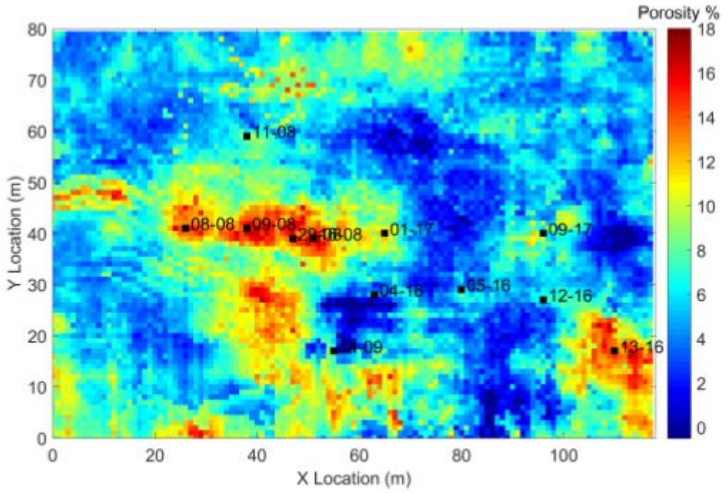

Figure 7.5: Mean map of all realizations

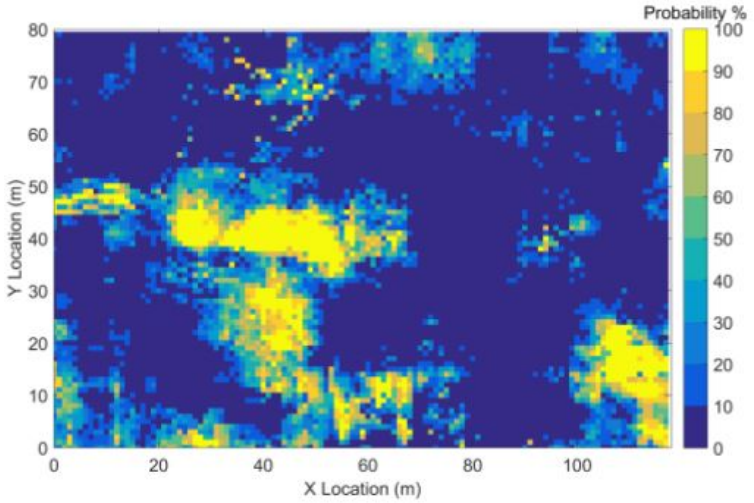

Figure 7.6: Probability map ($\phi > 10\%$)

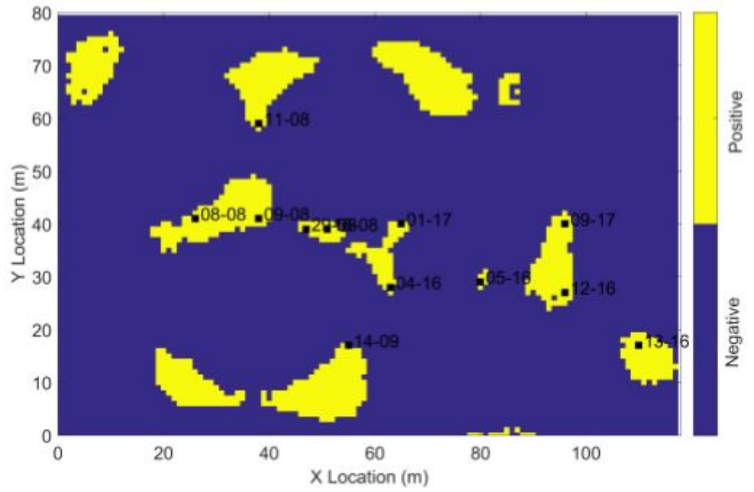

Figure 7.7: Error = SGS-ROCK - SGS-LS

Figure 7.8 and Figure 7.9 show semi-variograms of 30 realizations generated by SGS-extended ROCK and SGS-LS. As discussed previously, SGS-extended ROCK produced a series of realizations honoring the prior information. However, realizations created by SGS-LS deviate from the prior information due to the significant differences of magnitude between primary and secondary variables.

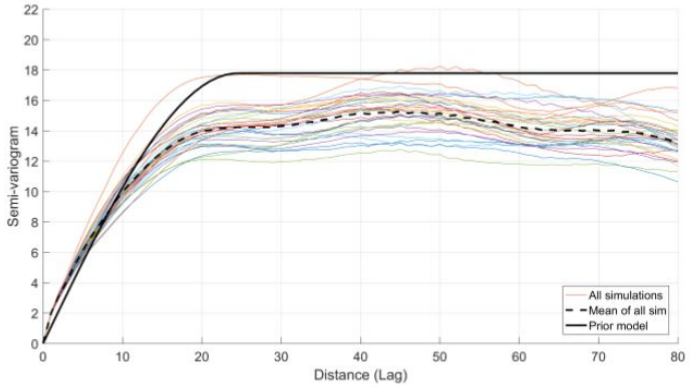

Figure 7.8: Variograms of realizations using SGS-ROCK

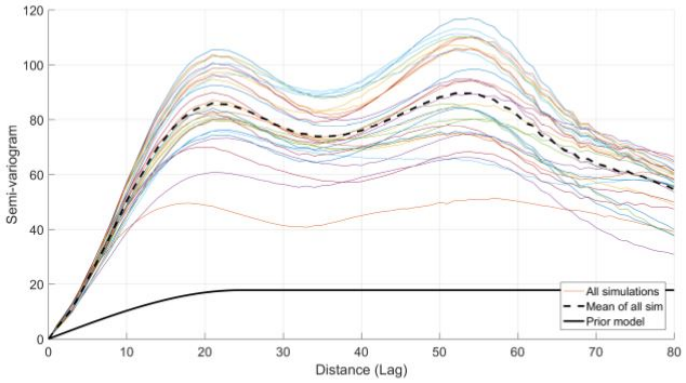

Figure 7.9: Variograms of realizations using SGS-LS

7.4 Conclusions

Sequential simulation is an effective tool for generating independent realizations for a second order stationary random field. In this study, a sequential simulation approach has been presented, which was implemented by the extended rescaled ordinary cokriging (ROCK) system. By pre-calculating the covariance lookup tables for primary and secondary datasets, and restricting the neighbourhood search method to be limited to the covariance matrix size, the sequential simulation with extended ROCK was made computationally efficient. Furthermore, compared to the least-squares approach, the constraint applied to the weights led to a more adaptable and accurate version of sequential simulation.

Chapter 8

Conclusions and future work

8.1 Conclusions

Geostatistical techniques, such as kriging, cokriging, and sequential simulation, have been used in this thesis to analyse and characterize reservoir properties using a spatial correlation model. These approaches not only predict interpolated values at the unsampled locations, but also provide a measure of uncertainty for predicted values. To summarize this thesis,

1. The kriging method was reviewed in Chapter 2. Kriging uses a weighted average of neighbouring samples to predict the value at a given location. The kriging weights are computed by semi-variogram, which defines the spatial relationship in all the sample data points over the estimate area. The advantages and disadvantages were discussed at the end of the chapter.

2. In Chapter 3, a testing method, called cross-validation, was demonstrated. Cross-validation is used to evaluate how generalized the model is to a new independent dataset. After fitting a model by training dataset(s), performance of a geostatistical models can be measured by validation dataset(s).

3. In Chapter 4, the cokriging method was compared to the kriging method. Cokriging is used to take advantage of the covariance between primary variable (well-log data lateral sampled sparsely) and secondary variable (seismic attribute lateral sampled densely). Both kriging and cokriging methods were applied to Black-foot 3C-3D dataset to predict porosity. Porosity can be one of the most difficult properties to estimate in spatial reservoir characterization because it is only sampled at well locations. Compared to the kriged map, the cokriged map was able to capture highly

detailed variations over the estimate area. In a performance evaluation between kriging and cokriging using the cross-validation technique, cokriging demonstrated a lower RMS error.

4. Based on the traditional cokriging method, a modified cokriging system which combines well logs and multiple secondary attributes was presented in Chapter 5. This technique has the potential to decrease the uncertainty and improve the definition of the predicted map. It was applied to predict a distribution and thickness map of a channel system. The results confirmed that, when compared to the traditional cokriging method, the modified cokriging system enhanced the lateral resolution of the channel and reduced the uncertainty of prediction due to the use of more seismic attributes.

5. In Chapter 6, an improved block cokriging system was introduced and applied to a producing shale gas reservoir for predicting the spatial distribution of total organic carbon (TOC). By analyzing the estimate created by traditional and improved block cokriging methods, this approach improved the accuracy of the estimate, reduces the risk of generating negative values, and stabilized the block cokriging system.

6. As deterministic methods, kriging and cokriging can only provide one predicted result, which has trouble preserving the natural variability of reservoir properties. The sequential simulation technique, implemented by an extended cokriging method, was presented. The conditional mean and variance in the posterior distribution were obtained using the extended cokriging system. The advantage is validated by review of the estimated error map. This indicates that sequential simulation using the extended geostatistics method can produce an more accurate map, especially when dealing with the data point that has the dramatical value difference from well control points.

8.2 Future work

There is a lot of future work that could make this thesis more complete. Here, I only highlight two key items:

1. Build anisotropic semi-variogram models that can reflect directionality in the depositional setting.

2. Use a neural network approach (Russell, 2004) that may offer an opportunity for the non-linear relationship between the primary variable and the secondary variables.

References

1. Ambrose, R.J., Hartman, R.C., Diaz Campos, M., Akkutlu, I.Y. and Sondergeld, C., 2010, January. New pore-scale considerations for shale gas in place calculations. In SPE Unconventional Gas Conference. Society of Petroleum Engineers.

2. Babak, O. and Deutsch, C.V., 2009, Improved spatial modeling by merging multiple secondary data for intrinsic collocated cokriging. Journal of Petroleum Science and Engineering,69(1), 9399.

3. Castagna, J. P., and S. W. Smith, 1994, Comparison of AVO indicators: A modeling: Geophysics, 59, 18491855.

4. Claerbout, J., 1992, Earth sounding analysis: processing versus inversion: Blackwell Science Publications.

5. Connolly, P., 1999, Elastic impedance: The Leading Edge, 18, 438452.

6. Dermanis, A., 1984, Kriging and collocation: A comparison. Manuscripta geodaetica,9(3), 159167.

7. Deutsch,C.V.,Journel,A.etal., 1998, Geostatisticalsoftwarelibraryandusersguide. OxfordUniversity Press, New York.

8. Doyen, P. M., 1988, Porosity from seismic data -a geostatistical approach: Geophysics, 53, 12631257.

9. Doyen, P. M., L. D. den Boer, and W. R. Pillet, 1996, Seismic porosity mapping in the ekofisk field using a new form of collocated cokriging: Presented at SPE Annual Technical Conference and Exhibition.

10. Duffaut, K., T. Alsos, N. F. Al-Najjar, H. Rogn, and M. Landre, 2000, Shear-wave elastic impedance: The Leading Edge, 19, 12221229.

11. Dumitrescu, C., and L. Lines, 2006, VP/VS ratio of a heavy oil reservoir from Canada: CSEG CWLS Convention.

12. Gonzalez, J., 2013. Determination of formation organic carbon content using a new neutron-induced gamma ray spectroscopy service that directly measures carbon. Unconventional Resources Technology Conference (URTEC).

13. Goodway W. and Tessman D.J., 2001, Blackfoot 3C-3D a VectorSeisTM Case History, CSE Extended Abstracts, p. 14-17.

14. Goovaerts, P., 1997, Geostatistics for natural resources evaluation: Oxford University Press.

15. Goovaerts, P., 1998, Ordinary cokriging revisited: Mathematical Geology, 30, 2142.

16. Guerrero, J., C. Vargas, and L. Montes, 1996, Reservoir characterization by multiattribute analysis: The orito field case: Earth Sciences Research Journal, 14, 173180.

17. Hansen, T.M., Journel, A.G., Tarantola, A. and Mosegaard, K.,2006, Linear inverse Gaussian theory and geostatistics. Geophysics,71(6), R101R111.

18. https://www.cs.cmu.edu/ schneide/tut5/node42.html

19. Isaaks, E. H., and Srivastava, R. M., 1989, An Introduction to Applied Geostatistics: Oxford University Press, New York.

20. Memarsadeghi, N. and D. Mount, 2007: Efficient implementation of an optimal interpolator for large spatial data sets. Proceedings of the 7th international conference on Computational Science, Part II, Springer-Verlag, Berlin, Heidelberg, 503510.

21. Li, J. Y., and X. Chen, 2008, Reservoir fluid identification based on seismic data: Acta Petrolei Sinica, 29, 235238.

22. Ligas, M. and Kulczycki, M.,2010, Simple spatial prediction-least squares prediction, simple kriging, and conditional expectation of normal vector. Geodesy and Cartography,59(2), 6981.

23. Loseth, H., Wensaas, L., Gading, M., Duffaut, K. and Springer, M., 2011. Can hydrocarbon source rocks be identified on seismic data?. Geology, 39(12), pp.1167-1170.

24. Matheron, G., 1965, Les Variables Rgionalises et Leur Estimation. Masson et Cie, Paris.

25. Marfurt, K. J., and R. L. Kirlin, 2001, Narrow band spectral analysis and thin bed tuning: Geophysics, 44, 326.

26. Neto, A.A., Mota, B.B., Belem, A.L., Albuquerque, A.L. and Capilla, R., 2016. Seismic peak amplitude as a predictor of TOC content in shallow marine sediments. Geo-Marine Letters, 36(5), pp.395-403.

27. Olea, Ricardo A.,1999, Geostatistics for Engineers and Earth Scientists. Springer

28. Qin*, X., Han, D.H. and Zhao, L., 2014. Rock physics modeling of organic-rich shales with different maturity levels. In SEG Technical Program Expanded Abstracts 2014 (pp. 2952-2957). Society of Exploration Geophysicists

29. Russell, B., D. Hampson, T. Todorov, and L. Lines, 2002, Combining geostatistics and multi-attribute transforms: A channel sand case study, Blackfoot oilfield: Journal of Petroleum Geology, 25, 97117.

30. Russell, B.H., 2004. The application of multivariate statistics and neural networks to the prediction of reservoir parameters using seismic attributes: Ph.D. thesis, University of Calgary.

31. Tarantola, A.,2005, Inverse problem theory and methods for model parameter estimation. siam.

32. Wackernagel H., 2003, Multivariate geostatistics: an introduction with applications. Springer, Berlin Heidelberg New York, pp 387.

33. Xu, H., Sun, J., Russell, B. and Innanen, K., 2015, Porosity prediction using cokriging with multiple secondary datasets. CSEG Geoconvention.

34. Xu, H., Russell, B. and Innanen, K.A., 2016 Determination of reservoir thickness and distribution using improved rescaled cokriging. In: SEG Technical Program Expanded Abstracts 2016, 29672971.

35. Zhu, Y., Xu, S., Payne, M., Martinez, A., Liu, E., Harris, C. and Bandyopadhyay, K., 2012. Improved rock-physics model for shale gas reservoirs. In SEG Technical Program Expanded Abstracts 2012 (pp. 1-5). Society of Exploration Geophysicists.